Eur. Phys. J. A **8**, 41–58 (2000)

THE EUROPEAN PHYSICAL JOURNAL A

Level structure of ^{123}Cs observed from ^{123}Ba decay and described using the IBFM and CQPC models

A. Gizon[1,a], B. Weiss[1,b], P. Paris[2], C.F. Liang[2], J. Genevey[1], J. Gizon[1], V. Barci[1,b], Gh. Căta-Danil[1,c], J.S. Dionisio[2], J.M. Lagrange[3], M. Pautrat[3], J. Vanhorenbeeck[4], Ch. Vieu[2], L. Zolnai[5], J.M. Arias[6], J. Barea[7], and Ch. Droste[8]

[1] Institut des Sciences Nucléaires, IN2P3-CNRS/Université Joseph Fourier, 38026 Grenoble-Cedex, France
[2] CSNSM, IN2P3-CNRS, Bt. 104, 91405 Campus Orsay, France
[3] Institut de Physique Nucléaire, IN2P3-CNRS, B.P. 1, 91406 Orsay-Cedex, France
[4] I.A.A. Université Libre de Bruxelles, Boulevard du Triomphe, 1050 Brussels, Belgium
[5] Institute of Nuclear Research, Pf. 51, 4001 Debrecen, Hungary
[6] Departamento de Física Atómica, Molecular y Nuclear, Universidad de Sevilla, Aptdo. 1065, 41080 Sevilla, Spain
[7] Departamento de Física Aplicada, ESII, Universidad de Sevilla, Sevilla, Spain
[8] Institute of Experimental Physics, Warsaw University, Hoża 69, 00681 Warsaw Poland

Received: 3 January 2000 / Revised version: 25 February 2000
Communicated by J. Äystö

Abstract. The decay of ^{123}Ba to ^{123}Cs has been studied with mass-separated sources. Singles spectra of γ-rays, X-rays and conversion electrons as well as $\gamma-\gamma-t$, $\gamma-e^--t$, and $X-e^--t$ coincidences were recorded. A level scheme of ^{123}Cs has been constructed including 26 new excited states and 82 transitions. The existence of a $I^\pi = 11/2^-$, $T_{1/2} = 1.7$ s isomer, bandhead of the $h_{11/2}$ band, is confirmed. Its excitation energy equals 156.3 keV. A new $T_{1/2} = 114$ ns isomer has been established at 232 keV using the in-beam recoil catcher technique. It is assigned to the $I^\pi = 9/2^+$ bandhead of the $\pi g_{9/2}$ band. Collective bands based on the $1/2^+$ ground state and first $3/2^+$ excited state are proposed. The level structure is described in the frame of the interacting boson-fermion and core-quasiparticle coupling models.

PACS. 21.10.Re Collective levels – 23.20.Lv Gamma transitions and level energies – 23.20.Nx Internal conversion – 21.60.Ev Collective models – 27.60.+j $90 \leq A \leq 149$

1 Introduction

Nuclei with neutron number $64 \leq N \leq 70$ and proton number $Z \leq 54$ were predicted to possess relatively flat potential-energy surfaces with respect to the quadrupole shape asymmetry parameter γ [1]. The light Cs isotopes were calculated as γ-soft with prolate quadrupole deformation at low-excitation energy [2,3]. For ^{123}Cs, with a quadrupole deformation $\beta_2 = 0.24$ [4], the 55th proton is expected to occupy positive-parity orbitals originating from the $d_{5/2}$, $g_{7/2}$ or $g_{9/2}$ shell-model states and a negative-parity orbital from the $h_{11/2}$ spherical subshell producing strongly coupled bands and a decoupled band, respectively.

Band structures related to some of these orbitals have been effectively observed in ^{123}Cs by in-beam γ-ray spectroscopy studies [3, 5-7]. Many in-beam data are available so far contrary to experimental results for low-lying low-spin levels which are relatively scarce [8-11]. As these low-spin data were not taken into account, the high-spin bands established from in-beam experiments were not well positioned in the existing level schemes and, most of the time, their lowest parts were missing.

We have undertaken a study to establish the spin, parity and excitation energy of low-lying states of ^{123}Cs, particularly of the intrinsic states on which the bands are based, knowing that the magnetic moment, spin-parity and half-life of the ground state of ^{123}Cs are $\mu = +1.377$ n.m., $I^\pi = 1/2^+$ and $T_{1/2} = 5.9$ min, respectively [12-14]. In this publication, new data on low-spin states in ^{123}Cs populated from the β^+/EC decay of ^{123}Ba ($T_{1/2} = 2.7$ min) are presented. The techniques employed in decay-studies and on-line experiments are explained in Sect. 2. The level structure of ^{123}Cs including twenty-six new excited states is described in Sect. 3 and interpreted in Sect. 4 using the interacting boson-fermion model and the core-quasiparticle coupling model.

[a] e-mail: gizon@isn.in2p3.fr
[b] *Present address*: Université de Nice, F-06108 Nice Cedex, France
[c] *Permanent address*: National Institute for Physics and Nuclear Engineering, R-769000 Bucharest, Romania

2 Techniques and experimental results

2.1 Decay studies

Experiments were performed at the Synchrocyclotron facility at Orsay. Mass-separated ^{123}Ba samples were produced at the ISOCELE2 separator. Thick molten lanthanum metallic targets were bombarded with ^{3}He beams of 280 MeV energy and 1 to 2 μA intensity. The barium activity was extracted and collected as stable and volatile BaF^{+} ions produced by introducing CF_4 inside the ion source of the isotope separator [15]. Thus the ^{123}Ba isotope was extracted at a mass $A = 142$ (123+19) without any simultaneous pollution of ^{123}Cs. The mass-separated samples collected on aluminized mylar tape were transported by an automatic tape-transport system to a low-background detection site. A description of the technical details is given in [16]. In order to adjust the extraction parameters for ^{123}Ba, direct γ-ray singles or multi spectra were analysed. Then samples collected during 300 seconds were used during 300 seconds for $\gamma-\gamma-t$ coincidence measurements with a low-energy and high resolution HP Ge and a 20% efficiency Ge detector. Coincidence events were recorded on tape and sorted off-line.

The barium activity collected on the mylar tape was also transported sequentially inside an electron magnetic selector installed at the ISOCELE facility. Conversion electrons in a large energy range were detected by a Si detector with typical energy resolution of 2 keV. The mechanical set-up associated with the selector was designed in order to install a coaxial Ge detector in front of a thin Be window, at approximately 35 mm of the radioactive sample. For a given magnetic field produced inside the magnetic selector eliminating e^{+} spectra, $\gamma - e^{-} - t$ coincidence events were recorded simultaneously with electron and γ-ray singles spectra.

The low-energy γ-ray spectrum recorded with the high-resolution Ge detector is shown in Fig. 1. Partial γ-ray and electron spectra are presented in Fig. 2. The $100-200$ keV energy range has been selected to show typical strongly converted M1, E2, or M1+E2 transitions at 116.2, 123.6, 137.0 and 201.0 keV compared to the weakly converted E1 transition at 120.0 keV.

Energies and intensities of the γ-rays assigned to the decay of ^{123}Ba to ^{123}Cs are listed in Table 1. The energies reported in the $50-100$ keV range have been obtained with the high-resolution Ge detector. As the collection and measurement times of 300 s used in the present studies are not very short in comparison to the $T_{1/2} = 5.9$ min half-life of the ^{123}Cs ground state, the associated decaying γ-rays have been identified as coincident events with the Xe K-X rays, in agreement with the results of [11,14]. The 61.7 keV γ-line reported as E3 in Table 1 corresponds to the decay of the $T_{1/2} = 1.7$ s,$(I^{\pi} = 11/2^{-})$ isomeric state in ^{123}Cs [11]. The internal conversion coefficients listed in Table 2 were determined using the 83.3, 97.3, 261.7, 304.0, 307.0 and 596.7 keV transitions in ^{123}Xe [11,14] as normalization lines. The α_K coefficients have been deduced from conversion electron singles spectra and conversion electron spectra in coincidence with Cs K_{α}+K_{β} X-rays.

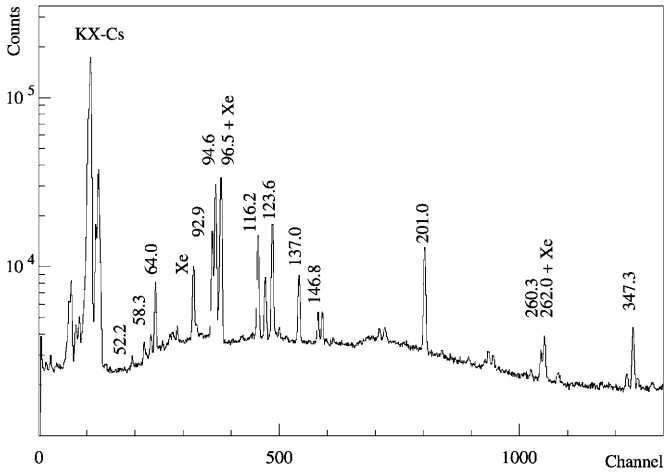

Fig. 1. Low-energy γ-ray spectrum observed in the decay of ^{123}Ba. The peaks produced in the subsequent ^{123}Cs to ^{123}Xe decay are indicated by "Xe"

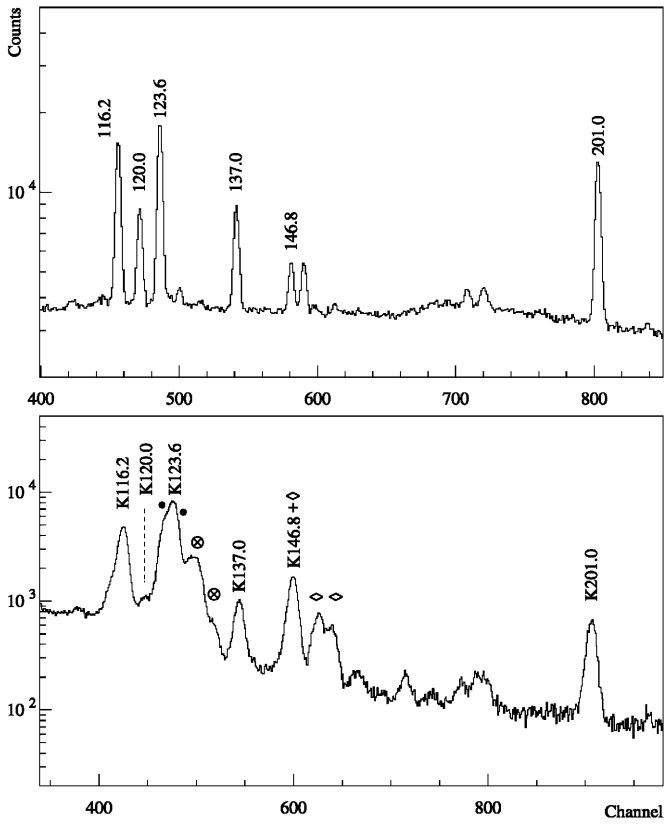

Fig. 2. Singles spectra recorded in the $100-200$ keV energy range with mass-separated samples of ^{123}Ba. γ-rays (*top*) and corresponding conversion electron lines (*bottom*) are selected to show differences in transition multipolarities. The symbols •,⊗,<> in the singles electron spectrum indicate the main L or M conversion lines of the strongest transitions at 92.9 and 94.6 keV in Cs, 97.3 keV in Xe, 116.2 and 123.6 keV in Cs, respectively

Table 1. List of γ-rays in ^{123}Cs with their energies in keV, relative intensities and placements between initial and final levels

$E_\gamma(\Delta E_\gamma)$	$I_\gamma(\Delta I_\gamma)$	Initial		Final	
(keV)	(relative)	E_i (keV)	I_i^π	E_f (keV)	I_f^π
23.2(1)[a]	w[b]	146.8	$5/2^+$	123.6	$3/2^+$,$5/2^+$
29.0(1)[a]	w[b]	123.6	$3/2^+$,$5/2^+$	94.6	$5/2^+$
30.6[a]	-	30.6	$3/2^+$	0.0	$1/2^+$
52.20(5)	1.5(1)	146.8	$5/2^+$	94.6	$5/2^+$
58.30(5)	2.7(1)	214.6	$7/2^-$	156.3	$11/2^-$
61.70(5)[c]	w[b]	156.3	$11/2^-$	94.6	$5/2^+$
63.97(3)	16.6(1)	94.6	$5/2^+$	30.6	$3/2^+$
67.75(5)	1.1(1)	214.6	$7/2^-$	146.8	$5/2^+$
84.8(1)	2.5(2)	231.6	$7/2^+$	146.8	$5/2^+$
92.92(3)	47(1)	123.6	$3/2^+$,$5/2^+$	30.6	$3/2^+$
94.57(3)	100[d]	94.6	$5/2^+$	0.0	$1/2^+$
96.46(6)	11.3(3)	328.1	$5/2^+$,$7/2^+$	231.6	$7/2^+$
108.1(1)	0.7(1)	231.6	$7/2^+$	123.6	$3/2^+$,$5/2^+$
116.2(1)	43.5(5)	146.8	$5/2^+$	30.6	$3/2^+$
120.0(1)	20(1)	214.6	$7/2^-$	94.6	$5/2^+$
123.6(1)	54.8(5)	123.6	$3/2^+$,$5/2^+$	0.0	$1/2^+$
137.0(1)	20.5(5)	231.6	$7/2^+$	94.6	$5/2^+$
146.8(1)	7.3(2)	146.8	$5/2^+$	0.0	$1/2^+$
201.0(1)	53(3)	231.6	$7/2^+$	30.6	$3/2^+$
231.7(2)	1.8(2)	698.8	$(7/2^+)$	467.6	$9/2^+$
233.5(2)	3.5(5)	328.1	$5/2^+$,$7/2^+$	94.6	$5/2^+$
236.0(2)	3.2(2)	467.6	$9/2^+$	231.6	$7/2^+$
260.3(1)	6.5(5)	474.9	$3/2^-$	214.6	$7/2^-$
262.0(2)	2.5(5)	494.0	$5/2^+$	231.6	$7/2^+$
309.5(3)	2.1(2)	784.4	$(5/2^-,7/2^-)$	474.9	$3/2^-$
336.2(3)	1.7(2)	811.2	$5/2^+$	474.9	$3/2^-$
347.3(2)	10.1(8)	494.0	$5/2^+$	146.8	$5/2^+$
351.3(3)	0.7(1)	474.9	$3/2^-$	123.6	$3/2^+$,$5/2^+$
370.6(2)	35(2)	494.0	$5/2^+$	123.6	$3/2^+$,$5/2^+$
373.1(2)	18.5(5)	467.6	$9/2^+$	94.6	$5/2^+$
380.3(5)	1.3(5)	474.9	$3/2^-$	94.6	$5/2^+$
389.0(5)	1.3(2)	621.0	$5/2^+$	231.6	$7/2^+$
399.6(2)	7.1(1)	494.0	$5/2^+$	94.6	$5/2^+$
401.3(2)	2.0(2)	524.7		123.6	$3/2^+$,$5/2^+$
410.8(2)	13.6(2)	557.5	$(5/2^+)$	146.8	$5/2^+$
428.3(3)	2.0(5)	1048.5	$5/2^+$	621.0	$5/2^+$
441.5(4)	2.6(5)	588.5		146.8	$5/2^+$
444.5(4)	3.0(3)	474.9	$3/2^-$	30.6	$3/2^+$
463.7(2)	6.3(3)	494.0	$5/2^+$	30.6	$3/2^+$
467.5(5)	2.2(3)	698.8	(7/2)	231.6	$7/2^+$
474.8(5)	1.6(2)	621.0	$5/2^+$	146.8	$5/2^+$
484.2(3)	6(1)	698.8	$(7/2^+)$	214.6	$7/2^-$
494.0(2)[e]	38.8(5)	494.0	$5/2^+$	0.0	$1/2^+$
		588.5		94.6	$5/2^+$
497.4(2)	16(2)	621.0	$5/2^+$	123.6	$3/2^+$,$5/2^+$
524.4(3)	5.8(5)	524.7		0.0	$1/2^+$
526.5(5)[e]	9.0(5)	621.0	$5/2^+$	94.6	$5/2^+$
		557.5	$(5/2^+)$	30.6	$3/2^+$
541.6(3)	6.0(5)	869.8		328.1	$5/2^+$,$7/2^+$
546.8(3)	8.9(5)	1021.5	5/2	474.9	$3/2^-$
557.4(5)	1.5(3)	557.5	$(5/2^+)$	0.0	$1/2^+$
569.8(3)	6.0(5)	784.4	$(5/2^-,7/2^-)$	214.6	$7/2^-$
590.4(3)	9.2(5)	621.0	$5/2^+$	30.6	$3/2^+$
602.8(5)	4.2(5)	749.7	$3/2^+$,$5/2^+$	146.8	$5/2^+$
621.0(3)	3.0(5)	621.0	$5/2^+$	0.0	$1/2^+$
626.3(3)	2.5(5)	749.7	$3/2^+$,$5/2^+$	123.6	$3/2^+$,$5/2^+$
633.5(5)	2.5(5)	728.0		94.6	$5/2^+$
635.1(4)	10.0(5)	866.7	$(5/2^+)$	231.6	$7/2^+$
664.5(5)	1.0(5)	811.2	$5/2^+$	146.8	$5/2^+$
670.6(3)	7.3(5)	817.2		146.8	$5/2^+$
673.8(5)	≈ 0.5	905.6		231.6	$7/2^+$
688.1(5)	2.5(3)	811.2	$5/2^+$	123.6	$3/2^+$,$5/2^+$
697.3(5)	≈ 0.5	728.0		30.6	$3/2^+$
716.6(3)	16.1(5)	811.2	$5/2^+$	94.6	$5/2^+$
718.8(3)[e]	22.5(5)	749.7	$3/2^+$,$5/2^+$	30.6	$3/2^+$
		866.7	$(5/2^+)$	146.8	$5/2^+$
723.1(5)	≈ 0.5	869.8		146.8	$5/2^+$
749.7(3)	5.0(5)	749.7	$3/2^+$,$5/2^+$	0.0	$1/2^+$
757.8(3)	2.1(2)	905.6		146.8	$5/2^+$
771.8(4)	1.0(3)	866.7	$(5/2^+)$	94.6	$5/2^+$
780.8(3)	6(1)	811.2	$5/2^+$	30.6	$3/2^+$
782.4(3)	3.0(3)	905.6		123.6	$3/2^+$,$5/2^+$
786.8(5)	0.9(2)	817.2		30.6	$3/2^+$
807.1(3)	2.5(1)	1021.5	5/2	214.6	$7/2^-$
811.0(2)[e]	7.5(5)	811.2	$5/2^+$	0.0	$1/2^+$
		905.6		94.6	$5/2^+$
816.8(3)[e]	2.0(2)	1048.5	$5/2^+$	231.6	$7/2^+$
		817.2		0.0	$1/2^+$
836.2(2)	2.0(2)	866.7	$(5/2^+)$	30.6	$3/2^+$
866.5(5)	2.0(5)	866.7	$(5/2^+)$	0.0	$1/2^+$
874.8(5)	1.3(5)	905.6		30.6	$3/2^+$
894.8(3)[f]	3.0(5)				
898.0(3)	2.7(5)	1021.5	5/2	123.6	$3/2^+$,$5/2^+$
905.5(5)	1.0(3)	905.6		0.0	$1/2^+$
932.3(5)[f]	1.7(4)				
956.0(5)[f]	2.9(3)				
991.3(4)	3.4(3)	1021.5	5/2	30.6	$3/2^+$
1017.0(10)	0.7(2)	1048.5	$5/2^+$	30.6	$3/2^+$
1021.9(6)	1.8(3)	1021.5	5/2	0.0	$1/2^+$
1048.5(10)	1.2(3)	1048.5	$5/2^+$	0.0	$1/2^+$

[a] Transition observed only in X-γ and e$^-$-γ coincidence spectra.
[b] Weak transition.
[c] E3 transition known from the decay of the $T_{1/2} = 1.7$ s isomer.
[d] Normalization.
[e] Doublet.
[f] Unplaced transition.

In many cases the K/L and L/M ratios were extracted from $\gamma - e^-$ coincidence spectra. The main prompt $\gamma - \gamma$ and $\gamma - e^-$ coincidence relationships are listed in Tables 3 and 4, respectively.

Table 2. Internal conversion electron data for transitions observed in the ^{123}Ba→^{123}Cs decay. This part of the table is for experimental and theoretical α_K coefficients and α_K/α_L ratios

E_γ(keV)	α_K				α_K/α_L				Multipolarity
	exp.	E1	M1	E2	exp.	E1	M1	E2	
64.0	3.5(4)	0.64	2.8	4.3	> 9	7.1	7.5	1.1	M1
92.9	0.85(4)	0.23	0.96	1.5	4.6(4)	7.4	7.5	2.1	M1+(E2)
94.6	1.2(1)	0.22	0.92	1.4	3(1)	7.4	7.5	2.1	E2+(M1)
96.5	0.66(8)	0.21	0.86	1.4	> 5	7.5	7.5	2.2	M1
108.1	1.1(2)	0.15	0.63	0.96		7.5	7.5	2.6	E2
116.2	0.65(7)	0.12	0.51	0.76	4.6(8)	7.5	7.5	2.8	M1+E2
120.0	0.11(2)	0.11	0.46	0.69		7.5	7.5	2.9	E1
123.6	0.41(2)	0.10	0.43	0.63	6.8(5)	7.6	7.5	3.0	M1+(E2)
137.0	0.35(5)	0.079	0.32	0.45	8(2)	7.6	7.6	3.3	M1+(E2)
146.8	0.32(3)	0.065	0.26	0.36	3.6(5)	7.7	7.6	3.6	E2
201.0	0.13(1)	0.027	0.11	0.13	4.7(2)	7.8	7.6	4.6	E2
236.0	0.067(15)	0.018	0.073	0.076		7.8	7.6	5.0	M1+E2
260.3	0.063(10)	0.014	0.056	0.056	5(1)	7.8	7.7	5.3	E2
347.3	0.036(6)	0.0065	0.026	0.023	6(1)	7.9	7.8	6.0	M1+E2
370.6	0.029(5)	0.0055	0.022	0.019	> 8	7.9	7.8	6.2	M1
373.1	0.025(4)	0.0054	0.022	0.018		7.9	7.8	6.2	M1+(E2)
389.0	0.030(10)	0.0049	0.020	0.016		7.9	7.8	6.2	M1
399.6	0.020(5)	0.0046	0.018	0.015	8(2)	8.0	7.8	6.3	M1+E2
401.3	0.026(10)	0.0045	0.018	0.015		8.0	7.8	6.3	M1+E2
410.8	0.016(2)	0.0043	0.017	0.014	8(2)	8.0	7.8	6.4	M1+E2
428.3	0.021(10)	0.0038	0.015	0.012		8.0	7.8	6.5	M1+E2
444.5	< 0.01[a]	0.0035	0.014	0.011		8.0	7.8	6.5	(E1)
463.7	0.011(3)	0.0032	0.013	0.010		8.0	7.8	6.6	M1+E2
484.2	0.004(2)[a]	0.0029	0.011	0.0087		8.0	7.8	6.7	E1
494.0[b]	0.0085(6)	0.0027	0.011	0.0087	8(2)	8.0	7.8	6.7	M1+E2
497.4	0.008(2)	0.0027	0.011	0.0080	6(2)	8.0	7.8	6.7	M1+E2
524.4	0.006(2)	0.0024	0.0094	0.0070		8.0	7.9	6.8	M1+E2
526.5	0.007(2)	0.0024	0.0093	0.0069		8.0	7.9	6.9	M1+E2
541.6	0.008(2)	0.0022	0.0087	0.0064		8.0	7.9	6.9	M1+E2
546.8	0.009(3)	0.0022	0.0085	0.0062		8.1	7.9	6.9	M1+E2
569.8	0.006(2)	0.0020	0.0076	0.0056		8.1	7.9	7.0	M1+E2
590.4	0.008(2)	0.0018	0.0070	0.0051	6(2)	8.1	7.9	7.1	M1+E2
621.0	0.005(2)	0.0016	0.0062	0.0045		8.1	7.9	7.1	M1+E2
670.6	0.005(1)	0.0014	0.0052	0.0037		8.1	7.9	7.3	M1+E2
716.6	0.0045(6)	0.0012	0.0044	0.0031	≈ 7	8.2	8.0	7.3	M1+E2
718.8[b]	0.0048(6)	0.0012	0.0044	0.0031	≈ 8	8.2	8.0	7.3	M1+(E2)

[a] Estimation from coincidence spectra.
[b] Doublet.

Table 2. Same as preceding but for experimental and theoretical α_L internal conversion coefficients

E_γ(keV)	α_L				α_K/α_L				Multipolarity
	exp.	E1	M1	E2	exp.	E1	M1	E2	
58.30	4.5(9)	0.12	0.49	6.2	<1	7.0	7.5	0.88	E2

2.2 On-line measurements

In order to search for short ^{123}Cs half-life isomers, additional in-beam gamma measurements were carried out using the recoil catcher method [17] and the CSNSM set-up at the Orsay MP-Tandem accelerator. A thin self-supported natural indium target of 400 μg/cm^2 thickness placed perpendicularly to the beam was bombarded by a ^{12}C beam (E = 57 MeV) pulsed every 400 ns (4 ns pulse width). The recoiling ions were collected on a thin (2 μm) aluminium catcher placed 7 cm downstream, this distance from the target corresponding to a time of flight of 27 ns. The catcher, with a central hole of 4 mm diameter made in order to minimize any reactions of primary ^{12}C ion beam with the aluminium catcher, was oriented at 45° relative to the beam direction. The burst of γ-rays

Table 3. Gamma-gamma coincidences observed in ^{123}Cs. All the γ-rays selected in the gates coincide with the Cs KX-rays and other γ-rays except for the 463.7 keV line which coincides only with Cs KX-rays. Weak coincidences are given between parentheses

Gate (keV)	Coincident γ-rays in keV placed in the level scheme
52.2	64.0, 94.6
58.3	260.3, 569.8
64.0	23.2, 52.2, 61.7, 84.8, 96.5, 120.0, 137.0, 233.5, 373.1, 399.6, 494.0, (569.8), 633.5, (718.8)
67.7	(64.0), 92.9, 94.6, 116.2, 123.6, 146.8, 260.3, 569.8
84.8	(52.2), (64.0), 92.9, 94.6, 116.2, 123.6, 146.8
92.9	23.2, 347.3, 370.6, 401.3, 410.8, 497.4
94.6	23.2, ($\approx$ 29), 52.2, 61.7, 84.8, 96.5, 120.0, 137.0, 233.5, 370.6, 373.1, 380.3, 399.6, 494.0, 526.5, 718.8
96.5	(52.2), 84.8, 92.9, 94.6, 137.0, 201.0, 231.7, 541.6
108.1	92.9, 94.6, 96.5, 123.6, (467.5), 541.6
116.2	67.7, 84.8, 96.5, 347.3, 410.8, 441.5, (541.6), 602.8
120.0	64.0, 94.6, 260.3, 484.2, 569.8
123.6	23.2, 67.7, 84.8, 108.1, (347.3), 370.6, (389.0), 401.3, 410.8, 497.4, 898.0
137.0	64.0, 92.9, 94.6, 96.5, 541.6, 635.1
146.8	67.7, 84.8, (96.5), 347.3, 410.8
201.0	96.5, 236.0, (467.5), 541.6, 635.1, 816.8
231.7	(96.5), 201.0
236.0	137.0, 201.0
260.3	58.3, (64.0), 67.7, (94.6), 120.0, (309.5), (546.8)
262.0	(137.0), (201.0)
347.3	92.9, 116.2, 123.6, 146.8
370.6	(29.0), 64.0, 92.9, 94.6, 123.6
373.1	64.0, 94.6
399.6 + 401.3	64.0, 92.9, 94.6, 123.6
410.8	92.9, (94.6), 116.2, 123.6, 146.8
463.7	KX-Cs
484.2	58.3, (67.7), (116.2), 120.0
^{D}494.0	64.0, 94.6
497.4	(29.0), 64.0, 92.9, 94.6, 123.6
^{D}526.5	(64.0), 94.6
541.6	(84.8), 92.9, 94.6, (96.5), (108.1)
569.8	58.3, 64.0, (67.7), 94.6, (116.2), 120.0, (146.8)
633.5 + 635.1	94.6, 116.2, 137.0, 201.0
670.6	(84.8), (92.9), (94.6), 116.2, 123.6
716.6	64.0, 94.6
^{D}718.8	(64.0), (94.6), 116.2, 146.8
780.8 + 782.4	(123.6)
811.0	(64.0), 94.6
^{D}816.8	(64.0), (92.9), (94.6), (123.6), 137.0, 201.0

^{D} Doublet.

Table 4. Gamma-electron coincidences observed in ^{123}Cs. Weak coincidences are given between parentheses

Gate (keV)	Coincident conversion-electron lines placed in the level scheme
64.0	$K_{52.2}$, L_{30}, M_{30}, $L_{61.7}$, $M_{61.7}$, $K_{120.0}$, $K_{137.0}$
84.8	$K_{92.9}$, $K_{96.5}$, $K_{116.2}$, $L_{92.9}$, $M_{92.9}$, $L_{116.2}$, $M_{116.2}$
92.9	$L_{30.6}$, $M_{30.6}$, ($K_{84.8}$), $K_{108.1}$, $L_{96.5}$, $M_{96.5}$, $K_{370.6}$
94.6	$K_{52.2}$, $L_{29.0}$, $K_{96.5}$, $K_{120.0}$, ($L_{96.5}$), $K_{137.0}$, $L_{137.0}$, $M_{137.0}$, $K_{233.6}$, $K_{236.0}$, $K_{370.6}$, $K_{373.1}$
96.5	L_{30}, M_{30}, $K_{84.8}$, $K_{94.6}$, $K_{108.1}$, $K_{116.2}$, $L_{94.6}$, $M_{94.6}$, $K_{137.0}$, $L_{137.0}$, $M_{137.0}$, $K_{201.0}$, $L_{201.0}$, (K_{231}), $M_{201.0}$
116.2	$L_{30.6}$, $M_{30.6}$, $K_{84.8}$, $L_{84.8}$, $K_{347.3}$
120.0	($K_{64.0}$), $L_{64.0}$, $K_{94.6}$, $L_{94.6}$, $M_{94.6}$, $K_{260.3}$
123.6	$K_{108.1}$, $L_{108.1}$, $K_{347.3}$, $K_{370.6}$, $K_{497.4}$
137.0	$L_{30.6}$, $M_{30.6}$, $K_{64.0}$, $L_{64.0}$, $K_{94.6}$, $L_{94.6}$, $M_{94.6}$, $K_{236.0}$, $L_{236.0}$
201.0	$L_{30.6}$, $M_{30.6}$, $K_{96.5}$, $L_{96.5}$, $M_{96.5}$, $K_{236.0}$, $L_{236.0}$
260.3	$L_{58.3}$, $K_{92.9}$, $K_{120.0}$, $L_{92.9}$, $K_{123.6}$, $L_{123.6}$, $K_{309.5}$
262.0	$K_{137.0}$, $K_{201.0}$, $L_{201.0}$, $M_{201.0}$
347.3	$K_{92.9}$, $K_{116.2}$, $L_{92.9}$, $K_{123.6}$, $L_{116.2}$, $K_{146.8}$, $M_{116.2}$, $L_{123.6}$, $L_{146.8}$
370.6	($L_{29.0}$), $K_{92.9}$, $L_{92.9}$, $K_{123.6}$, $M_{92.9}$, $L_{123.6}$, $M_{123.6}$
373.1	$L_{30.6}$, $L_{64.0}$, $K_{94.6}$, $L_{94.6}$, $M_{94.6}$
399.6	$L_{64.0}$, $K_{94.6}$, $L_{94.6}$, $M_{94.6}$
410.8	$K_{92.9}$, $K_{116.2}$, $L_{92.9}$, $K_{123.6}$, $L_{116.2}$, $K_{146.8}$, $M_{116.2}$, ($L_{123.6}$), $L_{146.8}$
494.0	$K_{94.6}$, $L_{94.6}$, $M_{94.6}$
497.4	$K_{92.9}$, $L_{92.9}$, $K_{123.6}$, $M_{92.9}$, $L_{123.6}$, $M_{123.6}$
^{D}526.5	$L_{64.0}$, $K_{94.6}$, $M_{64.0}$, $L_{94.6}$, $M_{94.6}$
541.6	$L_{64.0}$, $K_{94.6}$, $K_{96.5}$, $K_{116.2}$, $K_{146.8}$, $L_{116.2}$, $K_{201.0}$
569.8	$L_{58.3}$, $L_{64.0}$, $K_{94.6}$, $K_{120.0}$, $L_{94.6}$, $M_{94.6}$
602.8	$K_{92.9}$, $K_{116.2}$, $L_{92.9}$, $L_{116.2}$
633.5 + 635.1	($K_{94.6}$), $L_{94.6}$, $K_{116.2}$, $L_{116.2}$, $K_{137.0}$, $L_{137.0}$, $K_{201.0}$, $L_{201.0}$, $M_{201.0}$
664.5	$K_{116.2}$, $L_{116.2}$
670.6	($K_{92.9}$), $K_{116.2}$, $L_{92.9}$, $K_{123.6}$, $M_{92.9}$, $L_{116.2}$, $K_{146.8}$, $M_{116.2}$, $L_{146.8}$
716.6	$K_{64.0}$, $L_{64.0}$, $K_{94.6}$, $L_{94.6}$, $M_{94.6}$
^{D}718.8	$L_{30.6}$, $M_{30.6}$

^{D} Doublet.

following each heavy ion reaction was detected by a halo of six BaF_2 fast scintillators surrounding the target in coincidence with the HF oscillator of the pulsed beam. This halo started the measurements of the prompt γ-rays with the two Ge detectors installed close to the target on each side of the beam line. The same halo started also the measurement of the delayed gamma transitions with another Ge detector placed near to the catcher foil.

All the prompt transitions belonging to the bands based on the $I^{\pi} = 11/2^{-}$ and $9/2^{+}$ states were seen in the γ-ray spectra collected at the target position except

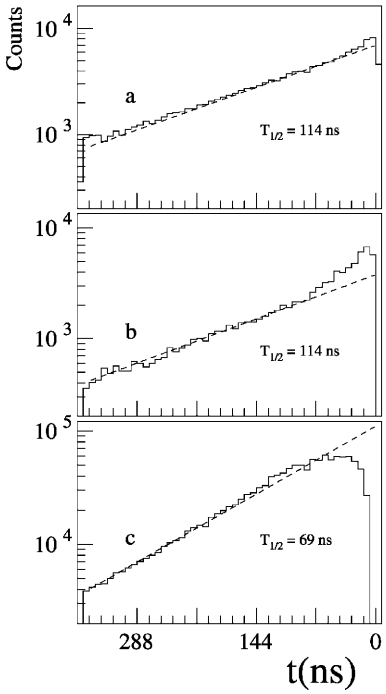

Fig. 3. Time spectra measured on-line in the In+^{12}C reaction at 57 MeV for γ-rays collected on the catcher (see details in Sect. 2.2). Curves a) and b) represent the experimental data obtained for the 201.0 and 137.0 keV γ-rays of ^{123}Cs, respectively. Curve c) is for the intense 89.5 keV line of ^{124}Cs produced in the same reaction. The $T_{1/2} = 69$ ns life time of this 89.5 keV line has been used as a reference

for the 137.0 and 201.0 keV transitions identified in previous in-beam measurements [3,6,7]. Moreover, in the delayed γ-spectra emitted by the catcher, all the prompt transitions disappear except for the 137.0 and 201.0 keV transitions which have significant contributions as well as all the known γ-rays coming from the decay of the ^{124m}Cs isomer ($T_{1/2} = 6.3$ s [18]). This shows the existence of a new ^{123}Cs isomer which had not been evidenced in previous in-beam measurements [6,7]. The half-life of this isomer ($T_{1/2} = 114\pm5$ ns) was deduced from the decay curves of the 137.0 and 201.0 keV delayed transitions (see Fig. 3) extracted from the $E_\gamma - T_\gamma$ matrix and compared to that of the 89.5 keV transition deexciting the long lived isomer ($T_{1/2} = 69$ ns) in ^{124}Cs (also produced by heavy ion induced reaction) identified previously at the ISOCELE facility [18].

3 The level scheme of ^{123}Cs

The ^{123}Cs level scheme obtained in the present work is shown in Figs. 4 and 5. The low-energy part displayed in Fig. 4 is presented to facilitate the discussion and the comparison with in-beam data. The excited states were placed on the basis of energies, intensities, multipolarities, and coincidence relationships of the transitions assigned to the decay of ^{123}Ba. The main difficulty in constructing the level scheme was caused by the existence of an intense and strongly converted 30.6 keV transition located in the γ-spectra in the vicinity of the Kα_2, Kα_1 and Kβ Cs X-rays at 30.62, 30.97 and 35.0 keV, respectively. The existence of this 30.6 keV transition in the ^{123}Ba$\rightarrow^{123}$Cs decay was already firmly established from the first multispectrum analysis of singles and X-β coincidence spectra recorded on mass-separated samples with a high-resolution Ge(Li) detector and a plastic β-counter [19]. The complexity of the level scheme has been solved thanks to $\gamma - e^-$ coincidences (Table 4). When gating on γ-rays, two groups of electrons were systematically observed at 25.0 and 29.4 keV corresponding to the L and M groups of the 30.6 keV highly-converted transition, respectively. Their intensity ratio $I_e(29)/I_e(25) \approx 0.2$ is in perfect agreement with the M/L ratio of conversion electrons of a 30.6 keV transition. At such an energy, the M/L ratio is almost independent of the multipolarity which explains why we have not established the multipolarity of the transition. Its placement just above the $I^\pi = 1/2^+$ ground state of ^{123}Cs is supported by the whole set of experimental results. We have measured M1 and E2 multipolarities for the 64.0 and 94.6 keV transitions, respectively (Table 2). The multipolarity of the 94.6 keV transition, cross-over of the 30.6 and 64.0 keV transitions, allows to assign spin and parity $3/2^+$ and $5/2^+$ to the two lowest excited states in ^{123}Cs as shown by the level schemes in Figs. 4, 5.

A $T_{1/2} = 1.7$ s,($I^\pi = 11/2^-$) isomer at 156.3 keV has been previously identified at the ISOLDE facility [11] as well as its decay mode to the ground state via the 61.7 keV, E3 transition. As a feeding of this isomer directly from the $I^\pi = 5/2^+$ ground state of ^{123}Ba is very unlikely and as we have observed the 61.7 keV γ-ray in our experiments, excited levels in ^{123}Cs situated above the isomer were populated by beta decay. These levels are identified at 214.6, 474.9 and 784.4 keV. Their spins and negative parity are proved by the E2, E1, E2 and M1/E2 multipolarities of the 58.3, 120.0, 260.3 and 569.8 keV transitions, respectively. This set of levels together with their connections to positive-parity levels are shown at the right-hand side of Fig. 4. Our results confirm the placement of the $I^\pi = 11/2^-$ isomer which was not considered in previous in-beam studies [6,7] and establish its internal feeding without any direct β/EC branching from the ^{123}Ba precursor.

The lowest $I^\pi = 9/2^+$ excited level in ^{123}Cs was proposed earlier [6,7] to be situated at an excitation energy of 296 keV, decaying to positive- and negative-parity low-lying states via an E2 transition of 201 keV and an E1 transition of 137 keV, respectively. A collective $\Delta I = 1$ band was based upon this $9/2^+$ state, including strong $I+1\rightarrow I$ γ-rays at 269, 304, 337, 368 .... keV. As mentioned in Sect. 2.2, the same prompt cascade was observed at the target position in our in-beam experiment performed with a pulsed beam at the MP-Tandem facility at Orsay, while the two decaying γ-lines at 137.0 and 201.0 keV were only seen as delayed lines at the catcher placed 7 cm behind the target. Moreover these two γ-lines exhibit the same half-life of $T_{1/2} = 114$ ns (Fig. 3) and were de-

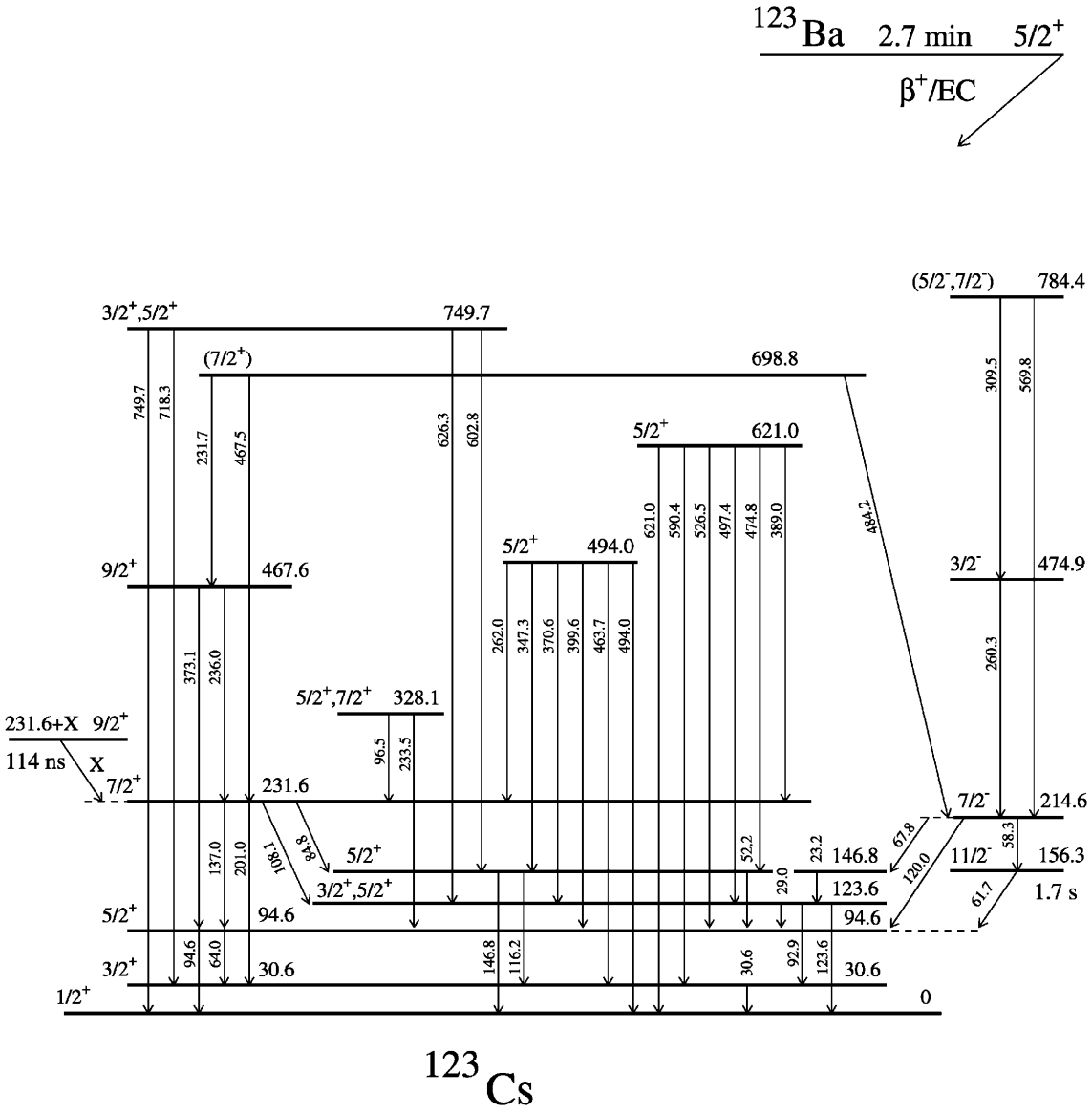

Fig. 4. Low-energy part of the level scheme of ^{123}Cs deduced from the ^{123}Ba ($T_{1/2}$ = 2.7 min) decay. Transition and level energies are given in keV

tected in the ^{123}Ba to ^{123}Cs decay with an intensity ratio $I_\gamma(137)/I_\gamma(201) = 0.38$ close to the value 0.49 reported earlier [7]. The E2 multipolarity deduced in the present work for the 201.0 keV transition (Table 2) agrees with the in-beam data [6,7] but the preponderant M1 character deduced from electron measurements and assigned to the 137.0 keV transition (Table 2) disagrees with these in-beam results in which it was supposed to be an E1 dipole transition. From these arguments, we conclude that there exists a $I^\pi = 7/2^+$ excited state in the level scheme of ^{123}Cs which deexcites to both the $I^\pi = 5/2^+$ state at 94.6 keV and $I^\pi = 3/2^+$ state at 30.6 keV (Fig. 4). Then, the $I^\pi = 9/2^+$ bandhead of a collective $\Delta I = 1$ band is located higher in energy than the $I^\pi = 7/2^+$ state at 231.6 keV, i.e. at $(231.6 + X)$ keV. It is not fed by beta decay in which the 137.0 and 201.0 keV transitions exhibit no long half-life . Very likely the $I^\pi = 9/2^+$ isomeric state with $T_{1/2}$ = 114 ns decays via a very low-energy isomeric transition to the $I^\pi = 7/2^+$ level at 231.6 keV. This would correspond to a situation similar to that known in ^{121}I and ^{119}I where short half-lives isomers are known [20, 21]. If the energy interval X between the $9/2^+$ (isomeric) and $7/2^+$ states is very small (e.g. few tenths of a keV), the $9/2^+ \rightarrow 7/2^+$ transition will not show up in the spectra. However a $(137.0 + X)$ keV transition should exist between the $9/2^+$ and $5/2^+$ levels, but it is not resolved from the known strong M1, $7/2^+ \rightarrow 5/2^+$ line of 137.0 keV.

The seventeen excited states reported in Figs. 4 and 5 with excitation energies larger than 470 keV have been established from coincidence and/or energy relationships. Except for four of them, they essentially decay to the $5/2^+$, $3/2^+$ and $1/2^+$ low-lying levels. In a few cases, one assigns tentatively spin and parity. The $I^\pi = 3/2^-$ state at

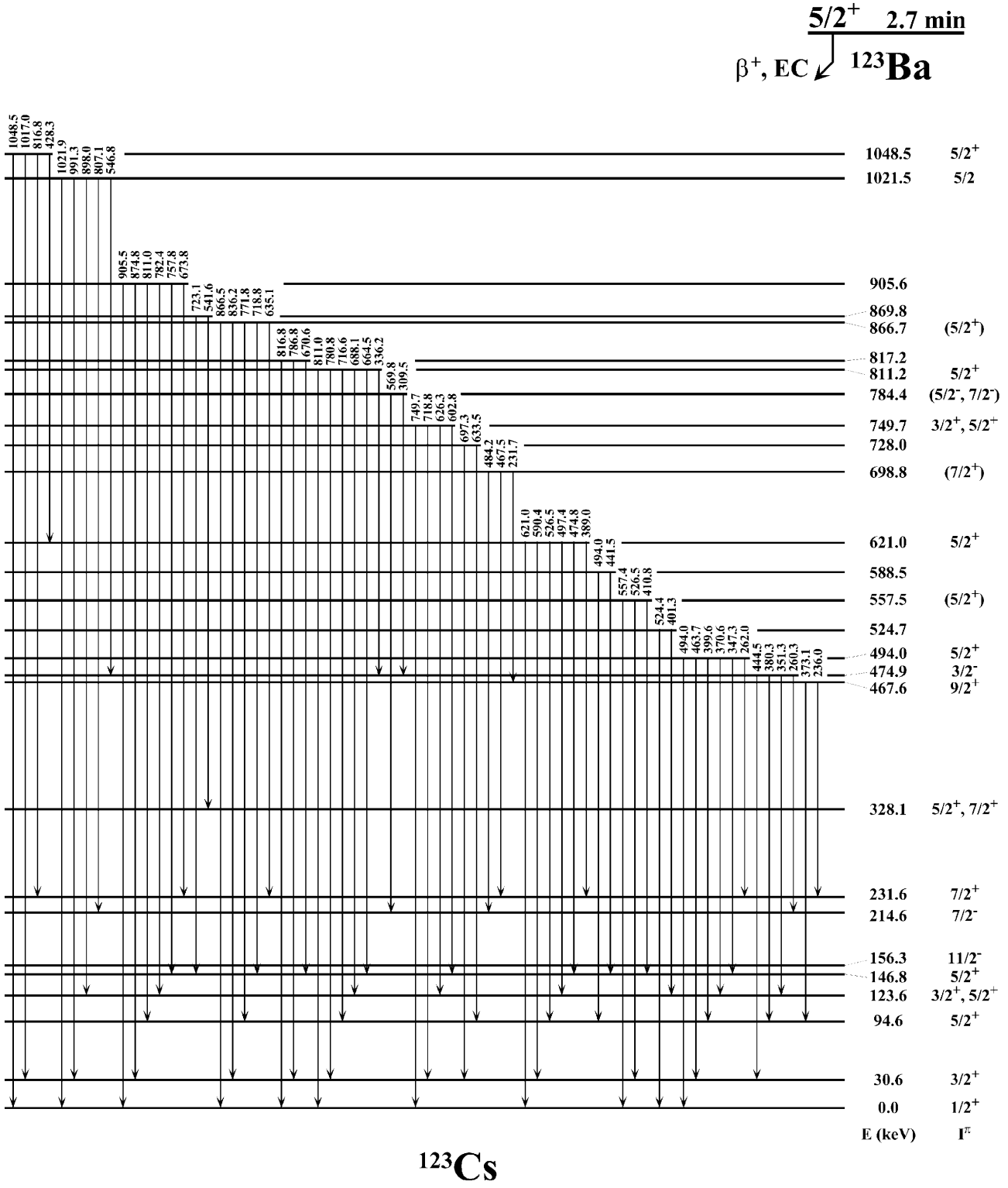

Fig. 5. Levels in ^{123}Cs populated in the ^{123}Ba ($T_{1/2} = 2.7$ min) decay. Gamma transitions are only shown from states having excitation energies larger than 400 keV. Transition and level energies are given in keV

474.9 keV belong to the negative-parity system built above the $I^\pi = 11/2^-$ isomeric state discussed above. Its main deexcitation goes to the $7/2^-$ state via the E2, 260.3 keV transition and also to three lowest positive-parity states. A possible E1 multipolarity for the 444.5 keV transition feeding the 30.6 keV state confirms the assigned negative-parity. The excited state at 698.8 keV which is weakly fed from ^{123}Ba decays mainly to the $7/2^-$ state at 214.6 keV via a 484.2 keV, E1 transition and also to the $7/2^+$ state at 231.6 keV and $9/2^+$ state at 467.6 keV via transitions of undetermined multipolarities. Spin and parity $7/2^+$ are proposed for the 698.8 keV state. A tentative $I^\pi = (5/2^-, 7/2^-)$ assignment has been retained for the state at 784.4 keV decaying via weak γ-rays to negative-parity states at 214.6 and 474.9 keV. The situation is not clear for the parity of the 1021.5 keV state. Indeed the M1/E2 character of the 546.8 keV γ-ray going to the $I^\pi = 3/2^-$ level at 474.9 keV indicates a negative parity while a β-branching of $\approx 2\%$ from ^{123}Ba suggests a positive parity. One could think of the existence of a doublet at ≈ 1021.5 keV if we knew the multipolarities of the 807.1, 898.0, 991.3, and 1021.9 keV lines (Fig. 5).

To confirm the spins and parities of the states shown in Figs. 4, 5, one can in principle estimate the (β^++EC) percentage feedings at each level from the γ-ray intensity balances. In the present case this procedure appears useless for two main reasons. First, the gamma intensity balance cannot be precisely estimated for the 30.6 keV level. Indeed, the collecting and counting times of 300 s used to study the ^{123}Ba samples were not adapted to normalize our results to the strong γ-line intensities known in the subsequent (β^++EC) decay of ^{123}Cs to ^{123}Xe, $T_{1/2} = 5.9$ min [11]. Second, in the present work levels have not been identified above 1.1 MeV but they could exist due to the high $Q(EC)$ value. However, assuming no feeding from the $I^\pi = 5/2^+$ ground state of ^{123}Ba to the $I^\pi = 1/2^+$ ground state of ^{123}Cs and assuming that the feedings to eventual levels above 1.1 MeV are weak, (β^++EC)-feedings and log *ft* values have been calculated using the tabulated $Q_\beta = 5463$ keV value [22] and the Gove and Martin tables [23] assigning successively 10% or 20% of the total feeding to the $I^\pi = 3/2^+$ excited state at 30.6 keV. With this procedure, the deduced log *ft* values appear too large. For example the log *ft* value reaches 6.0 ± 0.2 for the well established $I^\pi = 5/2^+$ state at 94.6 keV which receives approximately 20% of the β-feeding. The use of recent experimental data, $Q(EC) = 5.33 \pm 0.10$ MeV from [24] and $Q(EC) = 5389 \pm 20$ keV from [25], which are very close to the tabulated ones do not affect the log *ft* values appreciably. So, unfortunately the log *ft* values cannot be used to support spin and parity assignments.

4 Discussion and comparison with theories

The present level scheme of ^{123}Cs essentially derived from (β^+/EC) decay contains new informations at low excitation energy and allows to place the rotational band structures observed in in-beam experiments by fixing the excitation energy of their bandheads. It shows a large density of new positive-parity states below 500 keV excitation energy, some of them being separated by only 20 or 30 keV. A systematics of low-lying positive-parity levels known in neutron-deficient odd-A Cs isotopes is shown in Fig. 6. Spin and parity assignments of the ground states have been deduced from atomic beam magnetic resonance (ABMR) experiments [12,13]. They have been used as a basis to built all the cesium level schemes and deduce the spin and parity of the excited states. When the excitation energy of the $11/2^-$ bandheads arising from the $1/2^-[550]$ Nilsson orbital of the $h_{11/2}$ proton subshell is known, this $11/2^-$ state is also shown in the figure. For ^{119}Cs and ^{121}Cs, collective $\Delta I = 2$ bands have been observed by in-beam studies [3,6] but the low excitation energy of their $11/2^-$ base state is still undetermined.

A Woods-Saxon single-particle diagram for protons in the discussed mass region is given in Fig. 7. It shows the relative positions of the orbitals close to the Fermi surface which originate from the $d_{5/2}$, $g_{7/2}$, $h_{11/2}$, $s_{1/2}$ and $d_{3/2}$ subshells. The $9/2^+[404]$ orbital which corresponds to the deeply bound $\pi g_{9/2}$ proton hole state observed in the odd-A, odd-Z nuclei in this region is also shown in this figure.

The impossibility to measure the quadrupole moments of $I = 1/2$ states prevents a direct estimation of the corresponding quadrupole deformations. This deformation has been calculated to be $\beta_2 = 0.24$ for the ^{123}Cs ground state [4]. For this value the positive-parity Nilsson configurations accessible for the 55th proton are $1/2^+[420]$ and $3/2^+[422]$ originating from the $d_{5/2}$ and $g_{7/2}$ subshells and $9/2^+[404]$ from the $g_{9/2}$ subshell (Fig. 7).

Calculations performed so far for the light odd-A cesiums do not describe the experimental results. For example, bandhead energy calculations [3] made for ^{119,121,123}Cs fail to reproduce the real situation. Indeed the $3/2^+$, $1/2^+$, $11/2^-$, $9/2^+$ bandheads are calculated with the same order in the three isotopes contrary to the experimental situation. This illustrates the difficulty to perform realistic calculations for these transitional odd-A cesiums with neutron numbers close to $N = 68$. The complexity of a theoretical description is confirmed by an evaluation made for the $A \approx 120 - 130$ mass region using combined potential-energy-surface and cranked shell-model calculations [33]. This treatment has predicted a prolate-oblate shape coexistence for nuclei with $Z \leq 56$ and $N \leq 68$ while oblate shapes are expected to be more stable for nuclei with $Z \leq 56$ and $N \geq 70$.

In the present work we have applied the Interacting Boson-Fermion Model (IBFM) and Core-QuasiParticle Coupling model (CQPC) to the neutron-deficient ^{123}Cs nucleus. In the following subsections detailed treatments and results are given successively for the negative- and positive-parity states.

4.1 The IBFM-2 model calculation

Extensive calculations of the energy of both the positive- and negative-parity levels and electromagnetic properties of odd-A Cs isotopes have been presented in 1985 in the

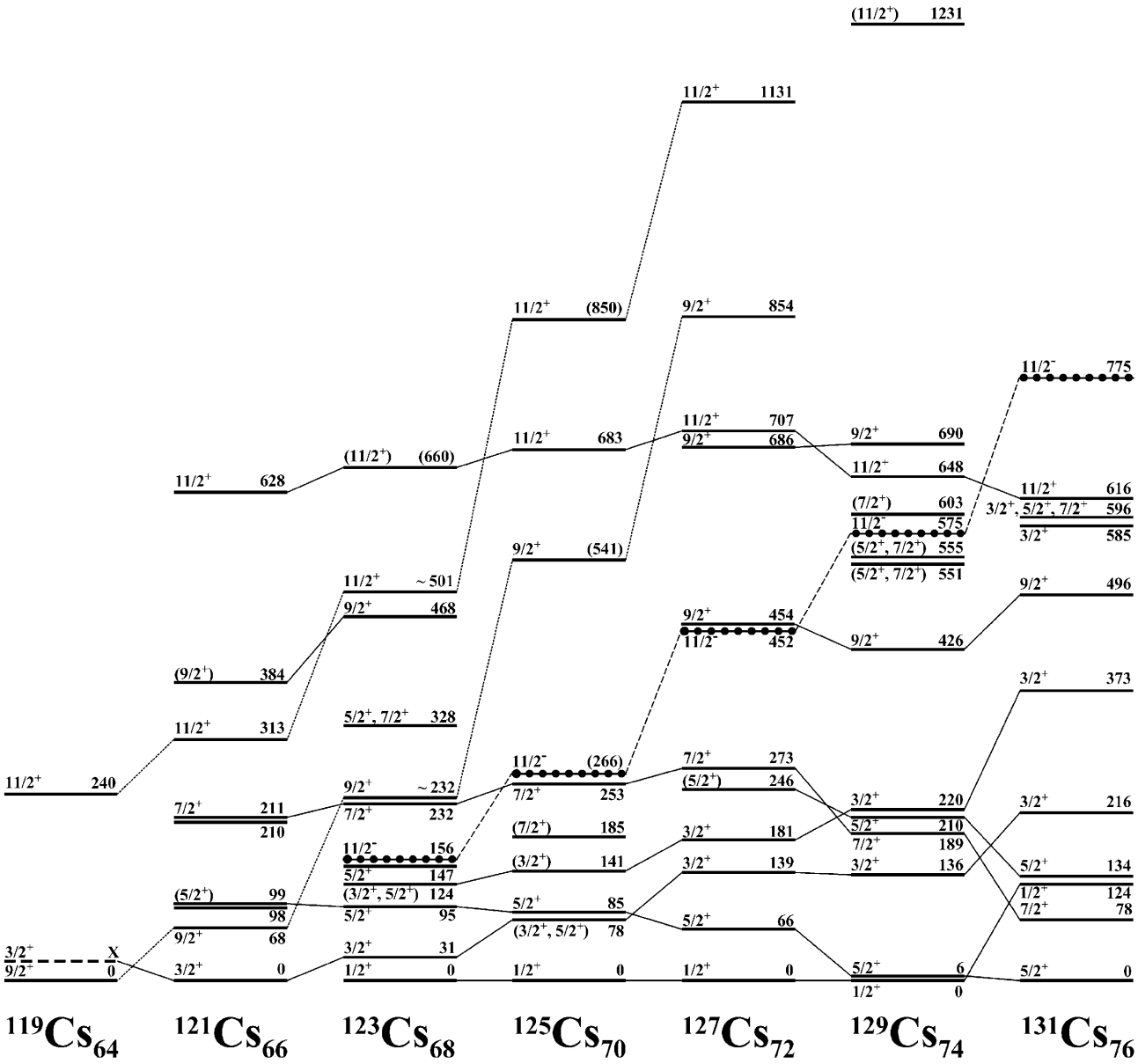

Fig. 6. Systematics of low-lying positive-parity levels in odd-A Cs isotopes. The evolution of the $I^{\pi} = 11/2^{-}$ state is also shown. The data are from the present work and [3,5-7,10,11,26-32]

framework of the IBFM-2 model [34]. At that time there was no reliable experimental information for the positive-parity states of Cs nuclei with mass lighter than $A = 125$ and these calculations had a full predictive character for the lighter isotopes and positive-parity states (see Fig. 3 of [34]). According to our knowledge, experimental data on positive-parity states emerging later [3,7] were never discussed in terms of any IBFM-like calculations while the negative-parity states in ^{125,127,129}Cs have been the subject of theoretical interpretations [35]. The IBFM-1 and IBFM-2 models are rather successful in describing energies and gamma branching ratios of the negative-parity states. This is well understandable due to the wealthier experimental information and a simpler structure due to the domination of the unique-parity $h_{11/2}$ orbital.

To describe the odd-proton nucleus ^{123}Cs in IBFM-2, an odd proton is coupled to the even-even core nucleus ^{122}Xe described in terms of proton- and neutron-bosons. The Hamiltonian is written as

$$H = H_B + H_F + V_{BF} \quad (1)$$

where H_B is the usual boson Hamiltonian for the even-even core described in the IBM-2 model, H_F the fermion Hamiltonian and V_{BF} the interaction between the odd-fermion and the bosonic core. For the boson core, ^{122}Xe, thirty-two levels up to spin $I = 16$ were calculated by using the parameters taken from [36] and given explicitly in Table 1 of [34] i.e. $\epsilon_\pi = \epsilon_\nu = 0.72$ MeV, $\kappa = -0.137$ MeV, $\chi_\pi = -0.80$, $\chi_\nu = -0.20$, $C_0^{(\nu)} = -0.05$ MeV and $C_2^{(\nu)} = -0.12$ MeV. The notations are those of [34]. It

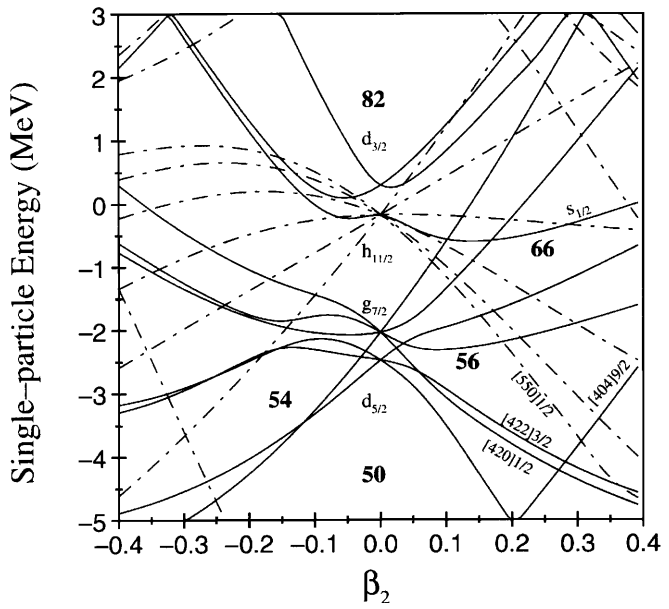

Fig. 7. Single-particle proton levels of the deformed Woods-Saxon potential as a function of the quadrupole deformation β_2. Positive- and negative-parity states are represented by solid and dot-dashed lines, respectively

Table 5. Single-particle energies ϵ_j, quasiparticle energies E_j and occupation probabilities v_j^2 for the single-proton orbitals considered in the calculations

Orbitals	s.p. energies (ϵ_j) MeV	q.p. energies (E_j) MeV	v_j^2
$g_{7/2}$	0.000	1.164	0.3159
$d_{5/2}$	0.200	1.251	0.2488
$h_{11/2}$	1.500	2.211	0.0639
$d_{3/2}$	3.000	3.595	0.0232
$s_{1/2}$	3.350	3.930	0.0193
$h_{9/2}$	7.000	7.507	0.0052
$f_{7/2}$	8.000	8.994	0.0036

is worth noting that these parameters are extracted from a systematic study of the Xe-Ba region and no attempt has been made to perform an individual fit to ^{122}Xe. The single-particle (s.p.) energies used and the corresponding BCS quantities are given in Table 5. The usual formulation of the boson-fermion interaction is used as given, for instance, in the study of ^{129,131}Ce [37].

We have calculated the level spectrum, the composition of the states in the single-particle orbitals and the E2 and M1 transition strengths for both the negative- and positive-parity states.

4.1.1 Negative-parity states

The $h_{11/2}$, $h_{9/2}$ and $f_{7/2}$ single-proton orbitals (Table 5) were considered for the negative-parity states. The adopted neutron-proton interaction strength parameters are $A_\pi = 0.0$ MeV (monopole), $\Gamma_\pi = 0.934$ MeV (quadrupole) and $\Lambda_\pi = 4.750$ MeV (exchange). The results of the calculations for the low-lying negative-parity states are shown in Fig. 8 together with the experimental spectrum.

The comparison of the calculated and experimental level schemes shows a good agreement. The $11/2^- - 7/2^-$ doublet made of the base state and first excited state is well reproduced by the calculations. This is not the case of the $15/2_1^- - 3/2_1^-$ doublet for which the relative position of the levels is inverted in the calculations. It appears that, relative to the experiment, the calculated level spectrum is stretched above 1 MeV excitation energy, the $17/2_1^-$ state being pushed about 300 keV upwards. The $I^\pi = (5/2^-, 7/2^-)$ level observed at 784 keV excitation energy, i.e. 628 keV above the $11/2^-$ bandhead, corresponds very likely to the $5/2_1^-$ level calculated 625 keV above the $11/2^-$ state, the experimental and theoretical branching ratios being in excellent agreement (Fig. 8).

The results of the calculations for the high-spin negative-parity levels are shown and compared to the experimental spectrum [5–7] in Fig. 9. The experimental energies of yrast states of the $h_{11/2}$ band with $\alpha = -1/2$ signature up to $I = 27/2$ are better reproduced than those of the $\alpha = +1/2$ states ($I = 17/2_1, 21/2_1, 25/2_1$) and yrare states ($19/2_2, 23/2_2$). This can be due to the fact that the γ-band of the core is calculated too high and to the truncation in the core states included in the calculation.

All the levels have a very pure $h_{11/2}$ configuration, the $h_{9/2}$ and $f_{7/2}$ components never exceeding 16% together. The high-spin levels of the $\alpha = +1/2$ and of the two $\alpha = -1/2$ branches are characterized by different dominant contributions of the core states in their wave functions which are shown below for the lowest level of each cascade:

$$\begin{aligned}
\left|11/2_1^-\right\rangle &= 33\%\left|0_1^+ \otimes h_{11/2}\right\rangle + 30\%\left|2_1^+ \otimes h_{11/2}\right\rangle \\
&\quad + 11\%\left|4_1^+ \otimes h_{11/2}\right\rangle + \ldots \\
\left|17/2_1^-\right\rangle &= \ 8\%\left|3_1^+ \otimes h_{11/2}\right\rangle + 38\%\left|4_1^+ \otimes h_{11/2}\right\rangle \\
&\quad + 29\%\left|6_1^+ \otimes h_{11/2}\right\rangle + \ldots \\
\left|19/2_2^-\right\rangle &= 38\%\left|4_2^+ \otimes h_{11/2}\right\rangle + 16\%\left|5_1^+ \otimes h_{11/2}\right\rangle \\
&\quad + 15\%\left|7_1^+ \otimes h_{11/2}\right\rangle + \ldots
\end{aligned}$$

In this schematic representation of the wave function, the numbers standing in front of kets give probabilities rather than amplitudes.

Bosonic effective charges $e_\pi^B = e_\nu^B = 0.12$ e.b [36], fermionic effective charge $e_\pi^F = 1.0$ e and boson gyromagnetic factors $g_\pi^B = 0.892$ μ_N and $g_\nu^B = 0.054$ μ_N [38] have been used to calculate electromagnetic transitions. For the radial integrals $< r^2 >$ the harmonic oscillator values have been taken. The spin g-factor has been quenched by a factor 0.7 as usual. The decay properties of the $15/2_1^-$ and $19/2^-1_1$ levels are well rendered by the theory. Indeed we have calculated the following transition probalities $B(\mathrm{E2};\ 19/2_1^- \rightarrow 15/2_1^-) = 0.505\ e^2b^2$ and $B(\mathrm{E2};\ 15/2_1^- \rightarrow 11/2_1^-) = 0.472\ e^2b^2$ which are close to the measured values $0.45^{+0.08}_{-0.04}\ e^2b^2$ and $0.40\pm0.02\ e^2b^2$,

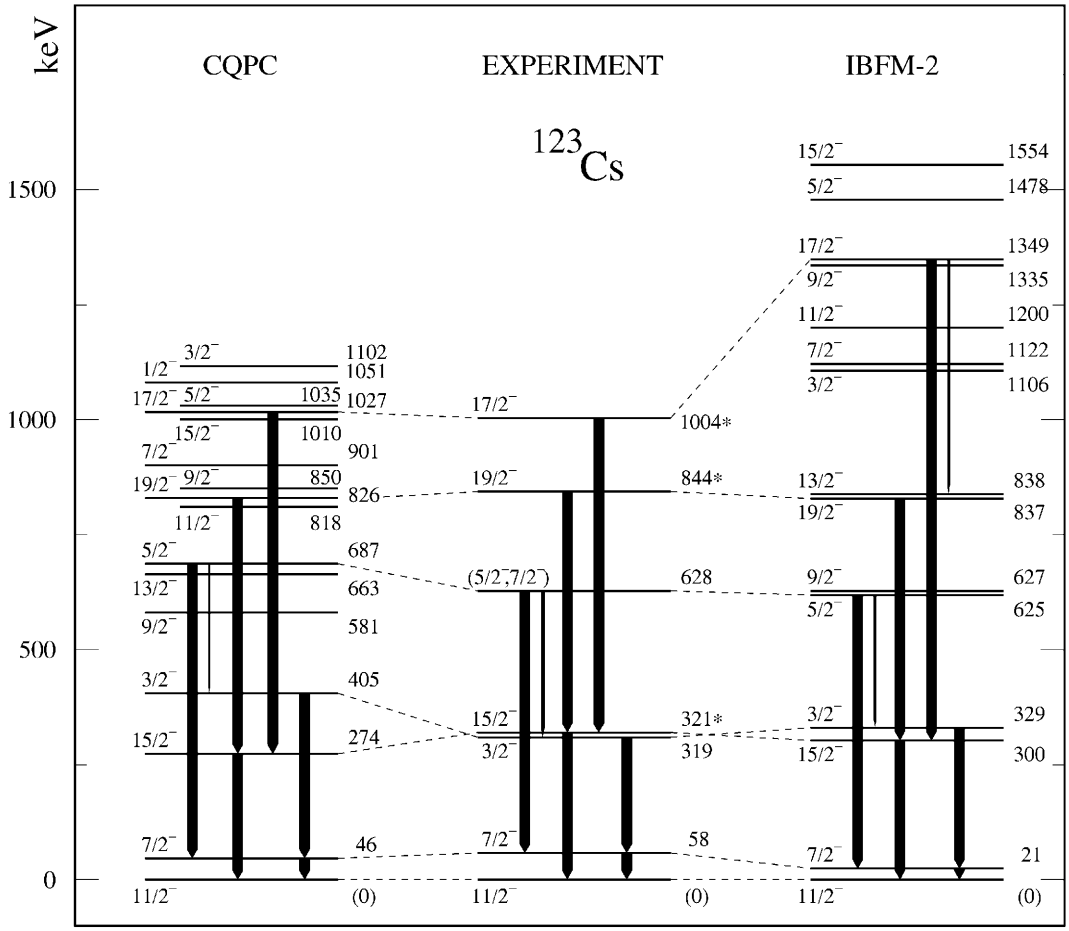

Fig. 8. Comparison of experimental *(middle)* and calculated low-spin negative-parity levels of ^{123}Cs. The experimental levels are those observed in the present work except the states labelled with an asterisk which were taken from in-beam data [5-7]. The levels calculated with the IBFM-2 model are shown in the *right* panel while those calculated with the CQPC model are represented in the *left* panel. For each level, the transition intensities are proportional to arrow widths, the strongest transition being set arbitrary to 100. Energies in keV are given relative to the first $11/2^-$ level which energy is set to zero

respectively [39]. The main decay properties of the high-spin states are reasonably well reproduced by the model (Fig. 9). The theoretical dipole magnetic moment of the $11/2^-_1$ state is $\mu(11/2^-_1) = 6.39\ \mu_N$. This value cannot be compared to the experimental one because this moment has not been measured but it agrees with $\mu = 6.55\pm0.10$ μ_N determined for ^{129}Cs [40].

To conclude, the negative-parity level spectrum is reasonably well described by the model.

4.1.2 Positive-parity states

We have performed calculations for the positive-parity states in ^{123}Cs with the IBFM-2 model using a procedure described in a previous analysis of positive-parity states of odd-A lanthanum isotopes [41]. In this multi-shell calculations, the $g_{7/2}, d_{5/2}, d_{3/2}$ and $s_{1/2}$ single-proton levels are considered for the fermionic part. Single-particle energies were taken originally from [42] but they had to be changed in order to reproduce the observed level density at low-excitation energy in ^{123}Cs (see Table 5). The energy separation between the $\pi g_{7/2}$ and $\pi d_{5/2}$ levels was reduced relative to that given in the above reference. This change has been needed to describe appropriately with the IBFM-1 model the odd-neutron Xe [43] and Ba isotopes [44]. For the odd-proton case, a similar change was already made to describe Eu isotopes using the IBFM-1 [45] and IBFM-2 [46] models. The neutron-proton interaction strengths $A_\pi = -0.035$ MeV, $\Gamma_\pi = 0.629$ MeV and $\Lambda_\pi = 0.746$ MeV are set by a best fit of the energy levels in ^{123}Cs.

Figure 10 shows that the experimental and calculated level energies are in good agreement. We discuss below the nature of the states and suggest band structures by comparing experimental and theoretical level spectra, branching ratios (Fig. 11) and components of the wave functions.

Experiments and IBFM-2 calculations agree about the $1/2^+$ spin and parity assignment to the ground state which has a wave function dominated by the $\pi d_{5/2}$ orbital with a 46% component. Large contributions (26% and 23%) in

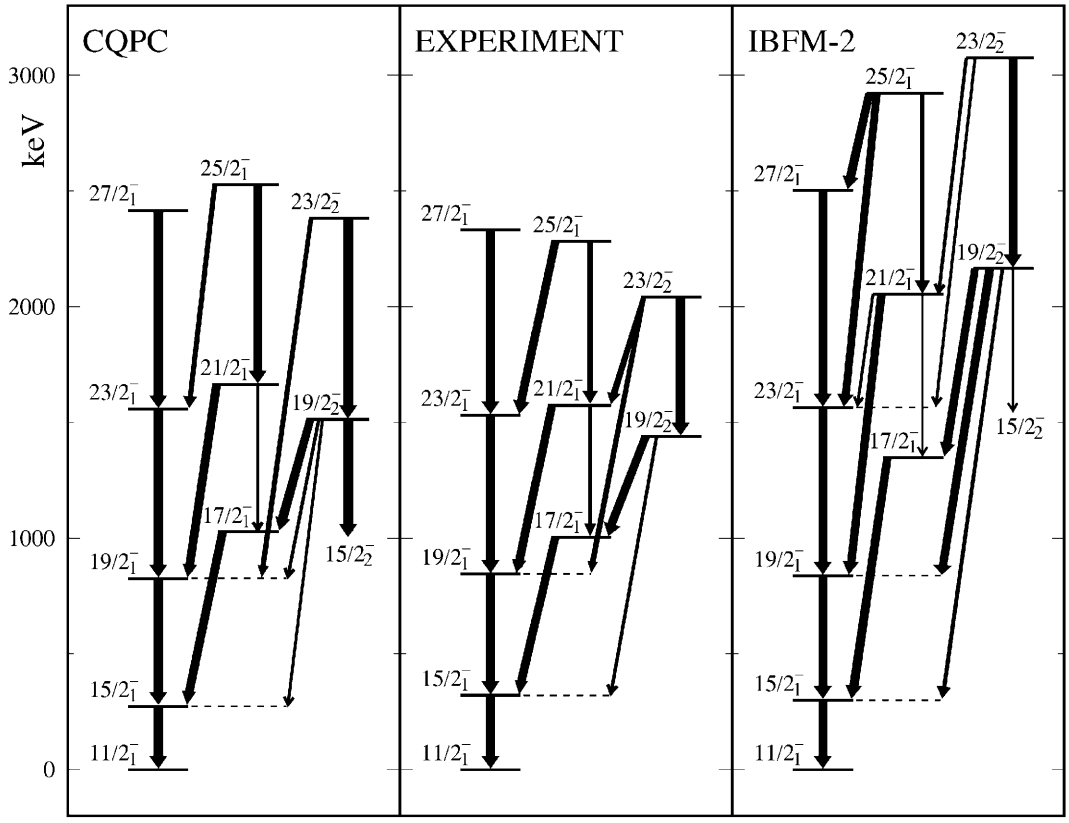

Fig. 9. The observed $h_{11/2}$ band structure in ^{123}Cs (*middle*) compared to calculated spectra obtained with the IBFM-2 model (*right*) and CQPC model (*left*). Only levels with $11/2 \leq I \leq 27/2$ are represented. To make the figure readable only the levels calculated which have their counterparts in the experiment [7] are shown. For each level, the transition intensities are proportional to arrow widths, the strongest transition being set arbitrary to 100. Energies in keV are given relative to the $11/2^-$ base level which energy is set to zero

the wave function arise from the $s_{1/2}$ and $d_{3/2}$ orbitals, respectively. This is somewhat surprising due to large energy spacings (≈ 3 MeV) between the $d_{5/2}$ s.p. level and the $s_{1/2}$ and $d_{3/2}$ s.p. levels. The ground state is associated with the $1/2^+[420](\pi d_{5/2})$ configuration as expected from the position of the Fermi level at a quadrupole deformation $\beta_2 \approx 0.24$ (Fig. 7). The calculated dipole magnetic moment for the ground state equals $\mu(1/2_1^+) = 1.79\ \mu_N$. It is compatible with the measured value 1.377(7) μ_N [13].

The first calculated excited state is $3/2_1^+$ and emerges from IBFM-2 with correct energy (30.6 keV experimental to compare to 36.9 keV calculated), spin and parity. It has a "dispersed" structure with $d_{3/2}$ (35%) and $d_{5/2}$ (33%) dominant components.

The second excited state located at 94.6 keV with $I^\pi = 5/2^+$ corresponds to the $5/2_1^+$ level calculated at 88.9 keV. Its wave function is strongly dominated by the $d_{5/2}$ component with an amplitude of 65%. The $9/2^+$ state observed at 468 keV which decays mainly to the $5/2_1^+$ level is assigned to the $\pi d_{5/2}$ band. Its counterpart calculated at 468 keV excitation energy is predicted to decay to both the $5/2_1^+$ and $7/2_1^+$ states but the intensity of the transition calculated towards the $7/2_1^+$ level is four times larger than the experimental one. Because of the strong experimental E2 transition observed between the $5/2_1^+$ level and the $1/2^+$ ground state, which is only partially reproduced by the calculations in spite of a dominant $d_{5/2}$ component (46%) calculated for the ground state, we propose to include the $1/2^+$ ground state into the $\alpha = +1/2$ signature branch and to consider the full band as being based on the $[420]1/2^+$ state. The state observed at 124 keV with $3/2^+$ or $5/2^+$ spin and parity assignments could correspond to the $3/2_2^+$ level calculated at 282 keV with a preponderant $d_{5/2}$ component (59%). Indeed the strong deexcitation observed for this level towards the $1/2^+$ ground state agrees with the model prediction. Then the 124 keV level would be the lowest member of the $\alpha = -1/2$ signature branch. The $7/2_3^+$ state calculated at 658 keV with a 50% $d_{5/2}$ component (Fig. 10) could be the second level in this branch predicted by the model, its experimental counterpart having not been observed.

The IBFM-2 calculations generate a clear band-like structure dominated by the spherical $\pi g_{7/2}$ orbital. It is represented from $5/2^+$ up to $15/2^+$ in the right hand-side panel of Fig. 10 with states having between 70% and 80% of $g_{7/2}$ component in their wave functions. The $5/2_2^+$ and $7/2_1^+$ levels calculated respectively at 173 and 190 keV are the counterparts of the $5/2_2^+$ and $7/2_1^+$ levels observed respectively at 147 and 232 keV. The calculated

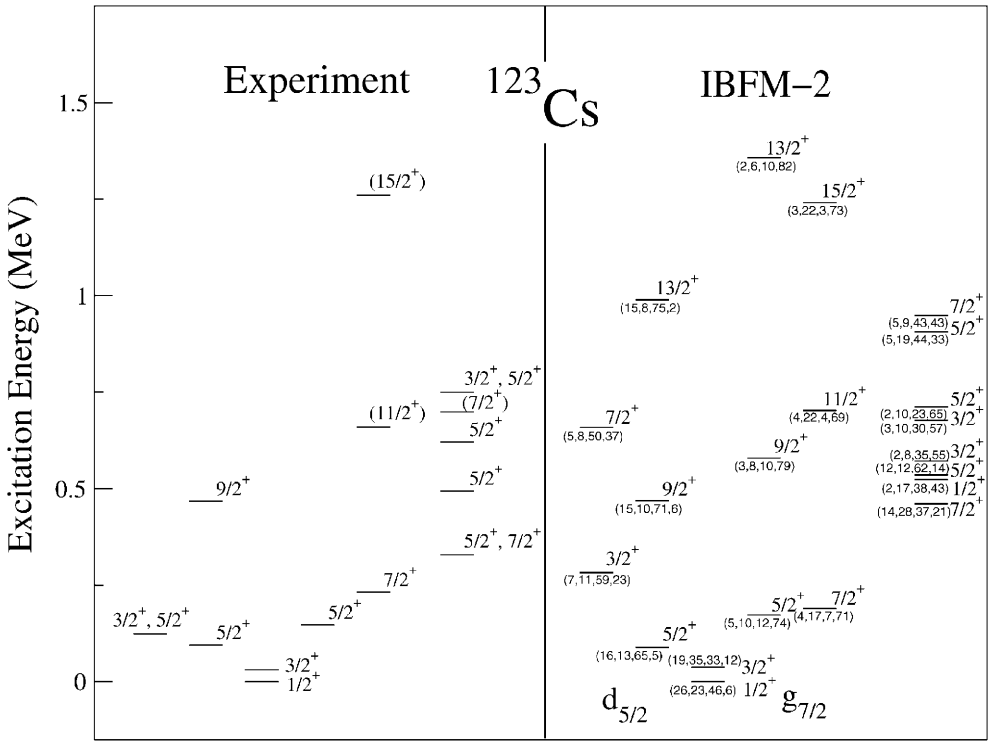

Fig. 10. Low-spin positive-parity levels in ^{123}Cs. The *left* panel shows the present experimental results which are compared to the theoretical predictions obtained with the IBFM-2 model (*right* panel). The experimental levels are those observed in the present work except for the $I^\pi = 11/2^+$ and $15/2^+$ levels taken from [7]. All the levels calculated below 1.0 MeV plus some selected ones above that energy are plotted together with the $s_{1/2}, d_{3/2}, d_{5/2}, g_{7/2}$ components of their wave functions

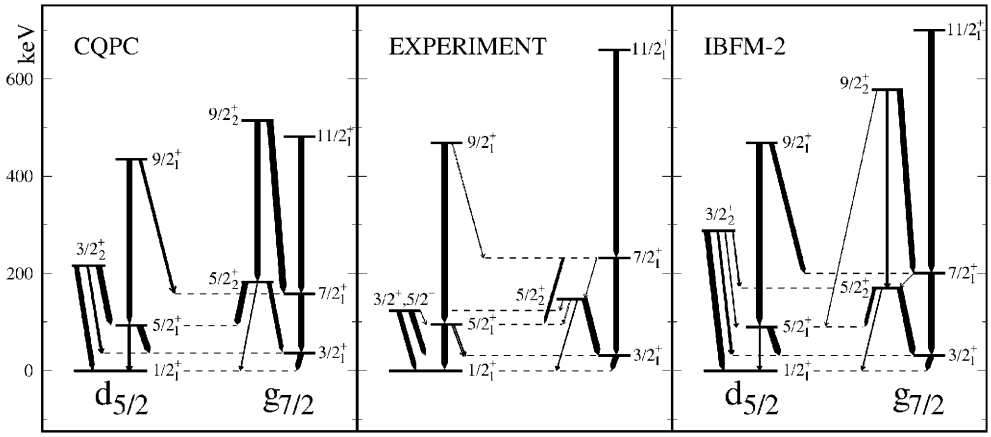

Fig. 11. Band structures of positive parity proposed for ^{123}Cs. The *middle* panel shows the present experimental results which are compared to the theoretical predictions obtained with the IBFM-2 model (*right* panel) and the CQPC model (*left* panel). For each state the transition intensities are proportional to arrow widths, the strongest transition being set arbitrarily to 100. The branching ratios can be directly deduced from arrow widths

and experimental branching ratios are similar except for the $5/2_2^+ \rightarrow 5/2_1^+$ transition which is overestimated in our IBFM-2 description (Fig. 11). The $9/2^+$ level of this band has not been observed in the experiments and is still unknown in this nucleus. The $7/2^+$ level is fed by the 428 and 600 keV γ-rays depopulating respectively the $(11/2^+)$ and $(15/2^+)$ levels [7]. We propose to include the 30.6 keV, $3/2_1^+$ level in the $\alpha = -1/2$ signature branch of the band because of the strong $7/2^+ \rightarrow 3/2^+$, E2 transition of 201.0 keV. As shown in Fig. 11, this band-like structure in ^{123}Cs is proposed to correspond to a $\pi g_{7/2}$ band. It fits into the systematics of the odd-A Cs nuclei shown in Fig. 6 and agrees with the observations made for odd-A La nuclei, in particular the isotone ^{125}La [47]. In ^{121}Cs, this $3/2_1^+$ state becomes the ground state. From ABMR and magnetic moment measurements it was identified as the $3/2^+[422]$ Nilsson state dominated by the spherical $\pi g_{7/2}$ subshell [12,13].

From this analysis we conclude that the observed positive-parity states are well explained by the IBFM-2 model.

4.2 The CQPC model calculation

The properties of the ^{123}Cs nuclei were also studied in the framework of the core-quasiparticle model developed in [48,49] and applied in numerous works, e.g. to the mass $A = 120 - 130$ region [39,47,50]. In the CQPC model, an odd-A nucleus is considered as an odd quasiparticle coupled to the neighbouring $(A-1)$ and $(A+1)$ even-even cores. In the case of the $^{123}_{55}$Cs nucleus it means that the 55th proton is coupled to the $^{122}_{54}$Xe and $^{124}_{56}$Ba cores. The valence particle/hole are coupled to the core due to quadrupole-quadrupole interaction. The pairing interaction is also taken into account.

The calculation shows that, to reproduce the ^{123}Cs data, one needs to increase significantly (about 40%) the strength of the core-particle quadrupole interaction comparing to the value used in [47,50]. To some extent this increment can simulate the effect of core polarization that can change the deformation of the core comparing with the deformation of the real neighbouring even-even nuclei. This problem would be elucidated if more properties of ^{123}Cs (e.g. E2 transition probabilities) sensitive to nuclear shape were known.

For the pairing interaction the standard formula $\Delta = 135/A$ MeV has been taken and the Fermi level position (in our case $\lambda - \epsilon(g_{7/2}) = -1.4$ MeV) was chosen to reproduce the number of valence protons in ^{123}Cs nucleus. The electromagnetic properties such as γ-transition probabilities and static magnetic moments have been calculated using standard values of proton charge and effective g-factors [47].

It was assumed that the collective states of the even-even cores (^{122}Xe and ^{124}Ba) can be described in the frame of the rigid triaxial rotor model of Davydov-Filippov. To simplify the problem we also assumed that both cores are identical. The calculations, which were pointed mainly to describe the negative-parity states, suggest a prolate core with parameters $\beta = 0.27$, $\gamma = 20^o$, $E(2^+) = 210$ keV[1]. It is worthwhile to mention that the corresponding parameters for the real ^{122}Xe and ^{124}Ba nuclei are $\beta = 0.295$, $\gamma = 24^o$, $E(2^+) = 331$ keV [39] and $\beta = 0.285$, $\gamma = 20^o$, $E(2^+) = 230$ keV, respectively. Thus, the accepted cores are more similar to the ^{124}Ba nucleus than to the ^{122}Xe nucleus. The thirty-three lowest core states up to $I^\pi = 16^+$ were used. The maximum spin of ^{123}Cs studied in this work is equal to 27/2.

4.2.1 Negative-parity states

The negative-parity states in ^{123}Cs were treated as the $\pi 1h_{11/2}$ and $\pi 2f_{7/2}$ orbitals coupled to the core collective states. The single-particle energies $\epsilon(h_{11/2}) = 2.18$ MeV and $\epsilon(f_{7/2}) = 7.18$ MeV were obtained from the Woods-Saxon potential [47]. The results of the CQPC calculations for the negative-parity states are presented in Fig. 8 and compared to experimental data. It follows from the calculation that the considered states are mainly built from the $h_{11/2}$ proton coupled to the core collective states. The decoupled band has a very pure $h_{11/2}$ configuration. The contribution of the competitive $\pi 2f_{7/2}$ state in the wave functions is lower than 10%. The $\pi 2f_{7/2}$ orbital has somewhat stronger influence on the low-spin low-energy states. For example, the $3/2^-_1$ level that is mainly (68%) composed of the 4^+_1 core state coupled to the $\pi 1h_{11/2}$ orbital has 14% contribution of the 2^+_1 state coupled to the $\pi 2f_{7/2}$ state. From the comparison made in Fig. 8 we see that the CQPC calculations reproduce all low-spin states observed in this work. The $I = (5/2^-, 7/2^-)$ state, observed at 784.4 keV, i.e. 628 keV above the $11/2^-$ level (Fig. 4), is too weakly fed in β-decay to obtain a unique I^π assignment. We propose that this state could correspond to the $I^\pi = 5/2^-_1$ state calculated at 687 keV. Indeed, the observed and calculated decay mode of the level to both the lowest $7/2^-_1$ and $3/2^-_1$ states are in good agreement, the branching ratio for the $5/2^-_1 \to 7/2^-_1$ and $5/2^-_1 \to 3/2^-_1$ transitions being 2.9 ± 0.4 from the experiment and 2.74 from the theory. The last value was calculated taking the theoretical B(E2) and B(M1) values and the experimental transition energies. These results obtained with the CQPC model are in good agreement with the experiment and IBFM-2 predictions.

The CQPC model reproduces also high-spin negative-parity states populated in heavy-ion reactions [5–7]. We found that the levels belonging to the $\alpha = -1/2$ decoupled band with spins and parity $I^\pi = 11/2^-_1$, $15/2^-_1$, $19/2^-_1$, ... (see Fig. 9) have their counterparts in our calculations. What is more, for the $15/2^-_1$ and $19/2^-_1$ levels, the B(E2; $19/2^-_1 \to 15/2^-_1$) = 0.52 e^2b^2 and B(E2; $15/2^-_1 \to 11/2^-_1$) = 0.48 e^2b^2 values are in a reasonable agreement with the experimental ones [39] equal to $0.45^{+0.08}_{-0.04}$ e^2b^2 and 0.40 ± 0.02 e^2b^2, respectively. It is worthwhile to notice that the calculated dipole magnetic moment for the $11/2^-_1$ level equals 6.10 μ_N. As pointed out in Sect. 4.1.1, the experimental value for ^{123}Cs is not known so far but the measurement done for ^{129}Cs [40] gives $\mu(11/2^-_1) = 6.55(10)$ μ_N. It agrees very well with the theoretical prediction. According to our calculations, the states $I^\pi = 19/2^-_2, 23/2^-_2, 27/2^-_2, \ldots$ referred to as band 4 in [7] have a dominant contribution of the $4^+_2, 6^+_2, 8^+_2, \ldots$ core states, respectively. All these states have a very strong $K = 2$ component. Hence, this second $\alpha = -1/2$ band can be treated as the γ-vibrational band built on the $\pi h_{11/2}$ orbital. The third band with $\alpha = +1/2$ and states $I^\pi = 17/2^-_1, 21/2^-_1, 25/2^-_1, \ldots$ has a similar character. Its lowest state $17/2^-_1$ is calculated 1027 keV above the $11/2^-$ base state vs. 1004 keV measured (Fig. 8). Its levels have contributions of the $K = 2$ states with spins $I = 3^+_1, 5^+_1, 7^+_1, \ldots$. The differences between the three above discussed bands can be seen considering the main components of the calculated wave function of the

[1] The Bohr convention for β and γ parameters is used.

three representative states:

$$\begin{aligned}\left|11/2_1^-\right\rangle &= 35\%\left|0_1^+\otimes h_{11/2}\right\rangle + 31\%\left|2_1^+\otimes h_{11/2}\right\rangle \\ &\quad + 13\%\left|4_1^+\otimes h_{11/2}\right\rangle + \dots \\ \left|17/2_1^-\right\rangle &= 23\%\left|3_1^+\otimes h_{11/2}\right\rangle + 22\%\left|4_1^+\otimes h_{11/2}\right\rangle \\ &\quad + 17\%\left|6_1^+\otimes h_{11/2}\right\rangle + \dots \\ \left|19/2_2^-\right\rangle &= 45\%\left|4_2^+\otimes h_{11/2}\right\rangle + 26\%\left|5_1^+\otimes h_{11/2}\right\rangle \\ &\quad + 7\%\left|7_1^+\otimes h_{11/2}\right\rangle + \dots\end{aligned}$$

As mentionned in Sect. 4.1.1, the numbers in front of kets give probabilities rather than amplitudes. One sees that the second band with $\alpha = -1/2$ built on the $19/2_2^-$ state has much stronger γ-vibrational character than the $\alpha = +1/2$ band based on the $17/2_1^-$ state. This character is more pronounced than deduced from the IBFM-2 model. To sum up the results of calculation for the negative-parity levels, we can ascertain that all considered states with $I \leq 27/2$ are explained in the frame of the model assuming the odd proton $(h_{11/2}, f_{7/2})$ coupled to the collective prolate core. The new experimental information presented in this work supports the conclusion of [7] that the low-lying collective oblate states suggested in theory [33] are not, up to now, observed in ^{123}Cs.

4.2.2 Positive-parity states

For the positive-parity states the $s_{1/2}$, $d_{3/2}$, $d_{5/2}$ and $g_{7/2}$ single-proton orbitals were taken into account. Their energies are the same as those used in the present work in the IBFM-2 model calculations (see Table 5). Additionally, we included the $\pi 1g_{9/2}$ orbital with energy $\epsilon(g_{9/2}) = -5.35$ MeV similar to that used in [47]. The energy was fitted to reproduce the $9/2^+(114$ ns) isomeric state (Fig. 4). In result, the calculated energy of the $9/2^+$ state is equal to 236 keV which agrees with the experimental one, $E = 232$ keV.

The results of the CQPC calculations for the positive-parity states are presented in Fig. 11. It is interesting to notice that this low-energy level scheme and decay properties are similar to that obtained in the IBFM-2 model although there are some differences. For example, we observe that in the CQPC calculation the order of the close lying $5/2_2^+$ and $7/2_1^+$ states does not agree with the experiment as well as the IBFM-2 calculation.

The main component of the wave function of the $1/2_1^+$, $5/2_1^+$, $3/2_2^+$ levels is $\pi d_{5/2}$ orbital with probability about 48%, 43%, 43%, respectively. It is in qualitative agreement with the IBFM-2 model analysis, see discussion in Sect. 4.1.2. A difference is observed for the $3/2_1^+$ state which in the CQPC calculation is built of the $g_{7/2}$ orbital (70%) instead of the "dispersed" structure with $d_{3/2}$ and $d_{5/2}$ components from the IBFM-2 model.

In the framework of the CQPC model the dipole magnetic moments of the low-lying states were calculated:

a: $\mu(1/2_1^+) = 1.27\ \mu_N$ which is very close to the measurement $1.377(7)\ \mu_N$ [13].
b: $\mu(3/2_1^+) = 0.77\ \mu_N$. There is no experimental value for ^{123}Cs but in the case of ^{121}Cs [13] the measured value equals $0.770(4)\ \mu_N$.
c: $\mu(9/2^+; \pi g_{9/2}^{-1}) = 5.13\ \mu_N$. There is no experimental information for ^{123}Cs but, in the case of ^{119}Cs and ^{121}Cs [13], the appropriate values equal 5.46(3) and 5.41(3) μ_N, respectively.

In all cases the agreement between theory and experiment is excellent.

5 Summary

The decay of ^{123}Ba to ^{123}Cs has been studied with mass-separated sources. A level scheme of ^{123}Cs including twenty six new excited levels has been constructed by using γ-ray and conversion electron detection techniques. The excitation energy of the $I^\pi = 11/2^-$, $T_{1/2} = 1.7$ s long-lived isomer is confirmed to be 156.3 keV. This fixes unambiguously the excitation energy of the bandhead of the $h_{11/2}$ band structure. A new $T_{1/2} = 114$ ns isomer has been established at 232 keV using the recoil catcher technique on-line. It is assigned to the $I^\pi = 9/2^+$ bandhead of the $\pi g_{9/2}$ collective band. A collective band based on the $1/2^+$ ground state is proposed. A new band is established on the first $3/2^+$ excited state by adding the present results and in-beam data.

Two theoretical approaches have been used to explain the observed level structure, namely the IBFM-2 and CQPC models. There is a fair agreement between the two theories and the experiment. The negative-parity states are generated mainly from the $\pi h_{11/2}$ orbital with small components from the $\pi h_{9/2}$ or $\pi f_{7/2}$ orbitals. From the energy and decay mode of the calculated $5/2_1^-$ state, we propose a $I^\pi = 5/2^-$ assignment for the level at 784.4 keV excitation energy. The high-spin band structure is reasonably well described by the two models. All observed negative-parity states with $I \leq 27/2$ are explained in the framework of the CQPC model assuming the coupling of an proton from the $h_{11/2}$ or $f_{7/2}$ orbitals to a triaxial core. This means that the states with oblate deformation suggested in theory [33] are, up to now, not observed in ^{123}Cs.

The positive-parity states, whose the structure is much more complex than the negative-parity levels due to the mixing of the $s_{1/2}, d_{3/2}, d_{5/2}, g_{7/2}$ proton orbitals have been analysed using both models. The models give similar results reproducing the main characteristics of the experimental level spectrum. The $\pi d_{5/2}$ and $\pi g_{7/2}$ bands are identified among the calculated levels based on the composition of their wave functions. Observed levels are proposed to belong to these configurations by comparing their energies and electromagnetic properties (γ-decay modes, dipole magnetic moments) to model estimates. The $1/2^+$ ground state and first $3/2_1^+$ excited level are characterized by strongly mixed wave functions.

We are indebted to the staffs of the Synchrocyclotron and MP-Tandem at Orsay for providing the beams and to Mr. J.P. Richaud for preparing the targets at ISN, Grenoble. One of us (Ch.D.) is very grateful to T. Morek, S.G. Rohoziński and J. Srebrny for valuable discussions. Gh.C.-D. thanks ISN, Grenoble for hospitality. This work was supported in part by the exchange programme between CNRS and the Hungarian Academy of Sciences and by the Spanish DGICYT under contract PB98-1111.

References

1. R. Bengtsson, P. Möller, J.R. Nix, J.Y. Zhang, Phys. Scripta **29**, 402 (1984)
2. R. Wyss, F. Lidén, J. Nyberg, A. Johnson, D.J.G. Love, A.H. Nelson, D.W. Banes, J. Simpson, A. Kirwan, R. Bengtsson, Nucl. Phys. A **503**, 244 (1989)
3. F. Lidén, B. Cederwall, P. Ahonen, D.W. Banes, B. Fant, J. Gascon, L. Hildingsson, A. Johnson, S. Juutinen, A. Kirwan, D.J.G. Love, S. Mitarai, J. Mukai, A.H. Nelson, J. Nyberg, J. Simpson, R. Wyss, Nucl. Phys. A **550**, 365 (1992)
4. P. Möller, J.R. Nix, W.D. Myers, W.J. Swiatecki, Atom. Data and Nucl. Data Tables **59**, 185 (1995)
5. N. Yoshikawa, J. Gizon, A. Gizon, J. Phys. Lett. **39**, L102 (1978)
6. U. Garg, T.P. Sjoreen, D.B. Fossan, Phys. Rev. C **19**, 217 (1979)
7. J.R. Hughes, D.B. Fossan, D.R. La Fosse, Y. Liang, P. Vaska, M.P. Waring, J.Y. Zhang, Phys. Rev. C **45**, 2177 (1992)
8. Ch. Droste, W. Neubert, S. Chojnacki, T. Morek, K.F. Alexander, Z. Wilhelmi, Nucl. Phys. A **192**, 595 (1972)
9. G. Beyer, R. Arlt, E. Hermann, A. Jasinski, O. Knotek, G. Musiol, H.G. Ortlepp, H.V. Siebert, J. Tyrroff, Nucl. Phys. A **260**, 269 (1976)
10. R. Arlt, A. Jasinski, W. Neubert, H.G. Ortlepp, Acta Phys. Pol. B **6**, 433 (1976)
11. G. Marguier, A. Charvet, J. Genevey, C. Richard-Serre, A. Knipper, G. Walter, the Isolde Collaboration, J. Phys. G: Nucl. Phys. **7**, 101 (1981)
12. C. Ekström, S. Ingelman, G. Wannberg, M. Skarestad, Nucl. Phys. A **292**, 144 (1977)
13. C. Thibault, F. Touchard, S. Buttenbach, R. Klapisch, M. de Saint Simon, H.T. Duong, P. Jacquinot, P. Juncar, S. Liberman, P. Pillet, J. Pinard, J.L. Vialle, A. Pesnelle, G. Huber, the Isolde Collaboration, Nucl. Phys. A **367**, 1 (1981)
14. S. Ohya, T. Tamura, Nucl. Data Sheets **70**, 531 (1993)
15. J.C. Putaux, J. Obert, L. Kotfila, B. Roussière, J. Sauvage, C.F. Liang, A. Peghaire, P. Paris, J. Giroux, the Isolde Collaboration, Nucl. Instr. and Meth. **186**, 321 (1981)
16. P. Paris, C.F. Liang, D. Lecouturier, M. Arianer, J. Obert, A. Carnetta, A. Ferro, J. Fournet, J.C. Putaux, J.L. Sarrouy, Nucl. Instr. and Meth. **186**, 91 (1981)
17. J.M. Lagrange, M. Pautrat, J.S. Dionisio, Ch. Vieu, J. Vanhorenbeeck, Nucl. Instr. and Meth. in Phys. Res. A **271**, 527 (1988)
18. B. Weiss, C.F. Liang, P. Paris, A. Peghaire, A. Gizon, Z. Phys. A **313**, 173 (1983)
19. D.D. Bogdanov, A.V. Demyanov, V.A. Karnaukhov, M. Nowicki, L.A. Petrov, J. Voboril, A. Płochocki, Nucl. Phys. A **307**, 412 (1978)
20. Y. Liang, D.B. Fossan, J.R. Hughes, D.R. La Fosse, T. Lauritsen, R. Ma, E.S. Paul, P. Vaska, M.P. Waring, N. Xu, Phys. Rev. C **45**, 1041 (1992)
21. S. Törmänen, S. Juutinen, R. Julin, A. Lampinen, E. Mäkelá, M. Piiparinen, A. Savelius, A. Virtanen, G.B. Hageman, Ch. Droste, W. Karczmarczyk, T. Morek, J. Srebrny, K. Starosta, Nucl. Phys. A **613**, 282 (1997)
22. G. Audi, A.H. Wapstra, Nucl. Phys. A **565**, 1 (1993) and A **595**, 409 (1995)
23. N.B. Gove, M.J. Martin, Nucl. Data Tables **10**, 205 (1971)
24. A. Osa, T. Ikuta, K. Kawade, H. Yamamoto, S. Ichikawa, J. Phys. Soc. Japan **65**, 928 (1996)
25. F. Ames et al., Nucl. Phys. A **651**, 3 (1999)
26. J. Genevey, G. Marguier, A. Charvet, C. Richard-Serre, A. Knipper, J. Crawford, in *Proceedings of the 4th International Conference on Nuclei far from Stability, Helsingör, 1981,* report CERN 81-09 , p.483
27. J.R. Hughes, D.B. Fossan, D.R. La Fosse, Y. Liang, P. Vaska, M.P. Waring, Phys. Rev. C **44**, 2390 (1991)
28. Y. Liang, E.S. Paul, N. Xu, D.B. Fossan, Phys. Rev. C **42**, 890 (1990)
29. K. Kitao, N. Oshima, Nuclear Data Sheets **77**, 1 (1996)
30. L. Hildingsson, W. Klamra, Th. Lindblad, F. Lidén, Y. Liang, R. Ma, E.S. Paul, N. Xu, D.B. Fossan, J. Gascon, Z. Phys. A **340**, 29 (1991)
31. Y. Tendow, Nuclear Data Sheets **77**, 631 (1996)
32. Sun Huibin, Liu Yunzuo, Hu Dailing, Zhou Jiewen, Li Yuan, Z. Phys. A **336**, 37 (1990)
33. N. Xu, Jing-ye Zhang, Y. Liang, R. Ma, E.S. Paul, D.B. Fossan, Phys. Rev. C **42**, 1394 (1990)
34. J.M. Arias, C.E. Alonso, R. Bijker, Nucl. Phys. A **445**, 333 (1985)
35. N. Yoshida, A. Gelberg, T. Otsuka, I. Wiedenhöver, H. Sagawa, P. von Brentano, Nucl. Phys. A **619**, 65 (1997)
36. G. Puddu, O. Scholten, T. Otsuka, Nucl. Phys. A **348**, 109 (1980)
37. A. Gizon, J. Genevey, D. Bucurescu, Gh. Căta-Danil, J. Gizon, J. Inchaouh, D. Barnéoud, T. von Egidy, C.F. Liang, B.M. Nyakó, P. Paris, I. Penev, A. Płochocki, E. Ruchowska, C.A. Ur, B. Weiss, L. Zolnai, Nucl. Phys. A **605**, 301 (1996)
38. M. Sambataro, O. Scholten, A.E.L. Dieperink and G. Piccitto, Nucl. Phys. A **423**, 333 (1984)
39. Ch. Droste, T. Morek, S.G. Rohozinski, D. Alber, H. Grawe and D. Chlebowska, J. Phys. G: Nucl. Part. Phys. **18**, 1763 (1992)
40. M.S. Dewey, H.E. Mahnke, P. Chowdhury, U. Garg, T.P. Sjoreen and D.B. Fossan, Phys. Rev.**18**, 2061 (1978)
41. A. Gizon, J. Genevey, B. Weiss, Gh. Căta-Danil, J. Gizon, D. Barnéoud, R. Béraud, D. Bucurescu, T. von Egidy, A. Emsallem, C.F. Liang, P. Paris, I. Penev, A. Płochocki, Z. Phys. A **359**, 11 (1997) and references therein
42. P. Mukherjee, R. Bhattacharay, I. Mukherjee, Phys. Rev. C **24**, 1810 (1981)
43. Gh. Cata-Danil, D. Bucurescu, A. Gizon, J. Gizon, J. Phys. G: Nucl. Part. Phys. **20**, 1051 (1994)
44. D. Bucurescu, Gh. Cata-Danil, N.V. Zamfir, A. Gizon, J. Gizon, Phys. Rev. C **43**, 2610 (1991)

45. O. Scholten, N. Blasi, Nucl. Phys. A **380**, 509 (1982)
46. C.E. Alonso, J.M. Arias, M. Lozano, J. Phys. G: Nucl. Phys. **14**, 877 (1988)
47. K. Starosta, Ch. Droste, T. Morek, J. Srebrny, D.B. Fossan, D.R. LaFosse, H. Schnare, I. Thorslund, P. Vaska, M.P. Waring, W. Satuła, S.G. Rohoziński, R. Wyss, I.M. Hibbert, R. Wadsworth, K. Hauschild, C.W. Beausang, S.A. Forbes, P.J. Nolan, E.S. Paul, Phys. Rev. C **53**, 137 (1996)
48. F. Dönau and S. Frauendorf, J. Phys. Soc. Japan **44**, 526 (1978) Suppl.
49. F. Dönau and U. Hagemann, Z. Phys. **A293**, 31 (1979)
50. T. Morek, K. Starosta, Ch. Droste, D. Fossan, G. Lane, J. Sears, J. Smith and P. Vaska, Eur. Phys. J. **A3**, 99 (1998)